Table 1. 肝炎ウイルスキャリア対策

a．(感染を知らないまま)潜在しているキャリア	
・肝炎ウイルス検査	検査の必要性 検査の機会の拡大(無料検査・出前検査) 対象者の拡大
b．患者としてすでに通院・入院しているキャリア	
・治療 ・治療効果などの情報提供 ・治療連携	医療費補助の運用 適切な治療への導入 専門医への受診 肝癌早期発見・治療プロトコール
c．(感染を知ったが)継続的な受診をしないままでいるキャリア	
・受診への動機づけ ・公費助成により見出されたキャリアの健康管理	現状把握と要因分析 医療機関受診率の把握 肝炎診療ネットワークへの連携
d．新規感染によるキャリア	
	感染予防対策 ワクチン キャリアの新規発生状況の把握と対策

感染を知らないまま潜在しているキャリア数の把握と肝炎ウイルスキャリア対策❍

前項に示した2つの大規模集団を元に得た年齢階級別HBV・HCVキャリア率と国勢調査人口を用いて，わが国におけるキャリア数の推計を行ったところ，2005年時点ではHBVキャリア推計数は，903,145人(95% CI：83.7-97.0万人)，HCVキャリア推計数は，807,903人(95% CI：68.0-97.4万人)となった[4]．この推計値，HBVキャリア数約90万人，HCVキャリア数約81万人は，検査前には自身が感染を知らなかった献血集団や肝炎ウイルス検診受検者集団におけるキャリア率を元に算出された数値であることから考えると，「感染を知らないまま潜在しているキャリア」の推計数に相当する．

社会における存在状態により肝炎ウイルスキャリア(肝炎ウイルスの持続感染状態にある人)を分類すると，「a. 感染を知らないまま潜在しているキャリア」，「b. 患者としてすでに通院・入院しているキャリア」，「c. 感染を知ったが受診しないでいる，あるいは継続受診にいたっていないキャリア」，「d. 新規感染によるキャリア」と大きく4分類される(Table 1)．わが国の肝炎ウイルスに持続感染しているキャリア数の全体を把握するためには，さらに「b」，「c」，「d」それぞれの数の把握(burden)が必要である．その大きさと社会における存在状態に応じて具体的なキャリア対策を講じることが効果的と考えられ，把握するための大規模調査や研究が行われているところである．

今後の肝炎ウイルスキャリア対策，ひいては肝癌対策として，「d. 新規感染によるキャリア」に対しては，肝炎ウイルスの新規感染の動向調査・従来の感染防止対策を継続すること，「a. 感染を知らないまま潜在しているキャリア」に対しては，肝炎ウイルス検査の必要性を周知し，家族を含んだ職域集団などの対象者の拡大を図り，対象集団ごとの検査機会の利便性を促進すること，「b. 患者としてすでに通院・入院しているキャリア」に対しては，肝炎治療に適した医療へのアクセス状況，最新の抗ウイルス療法の治療効果や肝癌早期発見のための検査プロトコールなどの情報提供の現

状，医療費補助の運用と効果の把握をすること，さらに「c．感染を知ったが受診しないままでいるキャリア」に対しては，その現状把握と要因分析を行うために，公費助成により見出されたキャリアの健康管理や医療機関受診状況の追跡調査を行うこと，が重要と考えられる[5]．

おわりに

わが国の社会生活全般における肝炎ウイルス感染の発生要因が徐々に減少し，若い世代におけるHBV キャリア率や HCV キャリア率は低い値を示すにいたっている．肝炎対策基本法(2009 年 12 月)を基盤として，すでに感染しているキャリアへの対策，具体的には，肝炎ウイルス検査の推進，肝疾患診療ネットワークの構築，新規治療法の開発などが積極的に進められている．

肝炎・肝癌対策をその病因論的また疫学的視点から捉えた場合，これまで行ってきた肝炎ウイルス感染の動向調査・感染防止対策を継続しつつ，社会における肝炎ウイルスキャリアの存在状態別にそれぞれの課題を掲げて具体的な対策を推進することが肝癌対策にとっても重要であるといえる．肝炎対策の先進国であるわが国は，肝癌対策の新たな局面を迎えていると考えられる．

文　献

1) 厚生労働省大臣官房統計情報部：平成 21 年人口動態統計，上巻，2009
2) 日本肝癌研究会：第 5 回～第 18 回全国原発性肝癌追跡調査報告，日本肝癌研究会事務局，1982-2009
3) 田中純子ほか：肝炎ウイルス検診受診者(2002.4-2007.3 受診群)を対象とした解析．平成 19 年度厚生労働省科学研究費補助金肝炎等克服緊急対策研究事業「肝炎状況・長期予後の疫学に関する研究」報告書，p1-6，2008
4) Tanaka J et al：Total numbers of undiagnosed carriers of hepatitis C and B viruses in Japan estimated by age- and area-specific prevalence on the national scale. Intervirology 54：185，2011
5) 田中純子：肝炎ウイルス感染状況・長期経過と予後調査及び治療導入対策に関する研究．厚生労働省肝炎等克服緊急対策研究事業「肝炎ウイルス感染状況・長期経過と予後調査及び治療導入対策に関する研究」平成 22 年度　総括報告書，p1-27，2011

Supplemental Material can be found at:
http://dmd.aspetjournals.org/content/suppl/2011/11/02/dmd.111.040923.DC1.html

1521-009X/12/4002-322–328$25.00
DRUG METABOLISM AND DISPOSITION
Vol. 40, No. 2
40923/3743170

DMD 40:322–328, 2012

Prediction of In Vivo Hepatic Clearance and Half-Life of Drug Candidates in Human Using Chimeric Mice with Humanized Liver[S]

Seigo Sanoh, Aya Horiguchi, Kazumi Sugihara, Yaichiro Kotake, Yoshitaka Tayama, Hiroki Ohshita, Chise Tateno, Toru Horie, Shigeyuki Kitamura, and Shigeru Ohta

Graduate School of Biomedical Sciences (S.S., A.H., Y.K., S.O.) and Liver Research Project Center, Hiroshima University, Hiroshima, Japan (C.T.); Faculty of Pharmaceutical Sciences, Hiroshima International University, Hiroshima, Japan (K.S., Y.T.); PXB Mouse Production Department (H.O.) and R&D Department (C.T.), PhoenixBio Co., Ltd., Hiroshima, Japan; DeThree Research Laboratories, Ibaraki, Japan (T.H.); and Nihon Pharmaceutical University, Saitama, Japan (S.K.)

Received August 5, 2011; accepted November 2, 2011

ABSTRACT:

Accurate prediction of pharmacokinetics (PK) parameters in humans from animal data is difficult for various reasons, including species differences. However, chimeric mice with humanized liver (PXB mice; urokinase-type plasminogen activator/severe combined immunodeficiency mice repopulated with approximately 80% human hepatocytes) have been developed. The expression levels and metabolic activities of cytochrome P450 (P450) and non-P450 enzymes in the livers of PXB mice are similar to those in humans. In this study, we examined the predictability for human PK parameters from data obtained in PXB mice. Elimination of selected drugs involves multiple metabolic pathways mediated not only by P450 but also by non-P450 enzymes, such as UDP-glucuronosyltransferase, sulfotransferase, and aldehyde oxidase in liver. Direct comparison between in vitro intrinsic clearance ($CL_{int,in\ vitro}$) in PXB mice hepatocytes and in vivo intrinsic clearance ($CL_{int,in\ vivo}$) in humans, calculated based on a well stirred model, showed a moderate correlation ($r^2 = 0.475$, $p = 0.009$). However, when $CL_{int,in\ vivo}$ values in humans and PXB mice were compared similarly, there was a good correlation ($r^2 = 0.754$, $p = 1.174 \times 10^{-4}$). Elimination half-life ($t_{1/2}$) after intravenous administration also showed a good correlation ($r^2 = 0.886$, $p = 1.506 \times 10^{-4}$) between humans and PXB mice. The rank order of CL and $t_{1/2}$ in human could be predicted at least, although it may not be possible to predict absolute values due to rather large prediction errors. Our results indicate that in vitro and in vivo experiments with PXB mice should be useful at least for semiquantitative prediction of the PK characteristics of candidate drugs in humans.

Introduction

It is important to predict human pharmacokinetics (PK) and metabolism of drug candidates in the preclinical stage of pharmaceutical development. Various approaches to predict human clearance (CL) with in vitro metabolic systems, such as human liver microsomes and hepatocytes, have been reported (Nagilla et al., 2006; Brown et al., 2007; Fagerholm, 2007; Stringer et al., 2008; Chiba et al., 2009; Hallifax et al., 2010) but with limited success. One of the reasons for the discrepancy between predicted and observed CL may be that the preparation, storage, and experimental treatment of hepatocytes alter the normal function of metabolic enzymes (Wang et al., 2005). Although this might be ameliorated by using fresh hepatocytes immediately after isolation from the liver, these are not readily available and in any case show considerable interindividual differences.

It has become possible recently to predict CL and half-life ($t_{1/2}$) by means of computational approaches and physiologically based modeling (Ekins and Obach, 2000; De Buck et al., 2007; Tabata et al., 2009; Paixão et al., 2010). Accurate prediction of human PK is a key issue for the development of new drugs, because many new drug candidates with diverse chemical structures are metabolized not only by cytochrome P450 (P450) but also by non-P450 enzymes, such as UDP-glucuronosyltransferase (UGT) and sulfotransferase (SULT). It is also necessary to take into account the effects of cell permeability, transporter-mediated uptake, and excretion (Chiba et al., 2009; Huang et al., 2010).

Chimeric mice with humanized liver (PXB mice; PhoenixBio Co., Ltd., Hiroshima, Japan) have been generated from urokinase-type plasminogen activator/severe combined immunodeficiency mice transplanted with human hepatocytes (Tateno et al., 2004). In these mice, approximately 80% of the hepatocytes are human. The expression levels and metabolic activities of P450 and non-P450 enzymes in

This work was supported by a Grant-in-Aid for Young Scientists (B) from Japan Society for the Promotion of Science [Grant 22790109]; and PhoenixBio, Co., Ltd.

Article, publication date, and citation information can be found at http://dmd.aspetjournals.org.

http://dx.doi.org/10.1124/dmd.111.040923.

[S] The online version of this article (available at http://dmd.aspetjournals.org) contains supplemental material.

ABBREVIATIONS: PK, pharmacokinetics; CL, clearance; AO, aldehyde oxidase; $CL_{int,in\ vitro}$, in vitro intrinsic clearance; $CL_{int,in\ vivo}$, in vitro intrinsic clearance; CL_{oral}, oral clearance; CL_t, total clearance; P450, cytochrome P450; DMSO, dimethyl sulfoxide; fu, plasma unbound fraction; h-hepatocytes, PXB mice hepatocytes; LC/MS/MS, liquid chromatography tandem mass spectrometry; NAT, *N*-acetyltransferase; PXB mice, chimeric mice with humanized liver; *Q*, hepatic blood flow; Rb, blood/plasma concentration ratio; RI, replacement index; SULT, sulfotransferase; $t_{1/2}$, half-life; UGT, UDP-glucuronosyltransferase; AUC_{iv}, area under the concentration versus time curve by intravenous administration.

livers of PXB mice with a high replacement index (RI) are similar to those of humans (Katoh et al., 2004, 2005), and human-specific metabolites are formed in PXB mice (Inoue et al., 2009; Kamimura et al., 2010; Yamazaki et al., 2010; De Serres et al., 2011). Thus, PXB mice could be a good in vivo model for predicting drug metabolism in humans.

However, quantitative methods for predicting PK parameters of humans from data in PXB mice have not been established yet. Therefore, we selected 13 model compounds that are metabolized by P450 and/or non-P450 enzymes in liver and compared the PK parameters in humans and PXB mice, using both in vitro and in vivo approaches, to evaluate the utility of this animal model for the prediction of human PK.

Materials and Methods

Chemicals. 6-Deoxypenciclovir and mirtazapine were obtained from Toronto Research Chemicals Inc. (North York, ON, Canada). Dapsone, lamotrigine, salbutamol, and sulindac were purchased from Sigma-Aldrich (St. Louis, MO). Diclofenac was purchased from Tokyo Chemical Industry Co. Ltd. (Tokyo, Japan). Fasudil was obtained from Tocris Bioscience (Bristol, UK). (*S*)-Naproxen was purchased from Cayman Chemical (Ann Arbor, MI). Ibuprofen, ketoprofen, and (*S*)-warfarin were purchased from Wako Pure Chemicals (Osaka, Japan). Zaleplon was kindly provided by King Pharm. Inc. (Bristol, UK). All of the other regents and solvents were commercial products of the highest available grade or analytical grade.

Animals. The present study was approved by the animal ethics committee and was conducted in accordance with the regulations on the use of living modified organisms of Hiroshima University. PXB mice (10–14 weeks of age) with human hepatocytes were prepared by the reported method (Tateno et al., 2004). Human hepatocytes of a donor (African-American boy, 5 years old) were obtained from BD Biosciences (San Jose, CA). PXB mice were housed in a temperature- and humidity-controlled environment under a 12-h light/dark cycle.

The RI was determined by the measurement of human albumin in blood collected from the tail vein. The RI was estimated by the correlation curve between the human albumin levels in mouse blood and determined by using human-specific cytokeratin 8/18-immunostained liver sections (Tateno et al., 2004). The RI values of PXB mice used in this study ranged from 73.4 to 93.4%.

Administration. Drug solution (5 ml/kg) was administered intravenously to PXB mice at 0.3 to 5 mg/kg body weight. Solutions of dapsone, diclofenac, 6-deoxypenciclovir, fasudil, ketoprofen, ibuprofen, mirtazapine, naproxen, salbutamol, and sulindac were prepared in saline. In the cases of ketoprofen, ibuprofen, naproxen, and sulindac, equivalent amounts of alkali were added. Dapsone solutions contained 10% dimethyl sulfoxide (DMSO), and mirtazapine solutions were prepared with 10% DMSO and equivalent amounts of hydrochloric acid. Lamotrigine, and zaleplon solutions were prepared with 10% DMSO and 10% polyethylene glycol 400 in saline. Equivalent amounts of hydrochloric acid also were added to the solutions of lamotrigine and zaleplon. Warfarin was formulated in 3% DMSO and 97% saline with an equivalent amount of sodium hydroxide.

Blood samples after dosing were collected from orbital veins of PXB mice at predetermined times using heparinized glass. These samples were centrifuged, and the plasma was stored at −30°C.

Determination of Drug Concentrations in Plasma. A 10 μl aliquot of plasma was added to 40 μl of acetonitrile or methanol containing an internal standard (carbamazepine, ketoprofen, or ibuprofen). The mixtures were centrifuged at 14,000*g* for 5 min, and the supernatant was subjected to liquid chromatography tandem mass spectrometry (LC/MS/MS).

Isolation and Purification of Hepatocytes from PXB Mice. Fresh hepatocytes were isolated from PXB mice (13–15 weeks of age) by means of the in situ collagenase perfusion method and purified as described previously (Yamasaki et al., 2010). PXB mouse hepatocytes (h-hepatocytes) contained approximately 7% mouse hepatocytes. We used h-hepatocytes purified by the use of 66Z rat IgG and magnetic beads bearing anti-rat IgG antibodies. The magnetic removal of mouse hepatocytes reduced the level of mouse hepatocytes to approximately 2% (in this study, the purity of human hepatocytes from PXB mouse hepatocytes ranged from 96.6 to 99.7% after purification). Cell viability of the hepatocytes used in the experiments ranged from 79 to 91%, as determined by means of the trypan blue exclusion test.

In Vitro Metabolic Studies Using h-Hepatocytes. The h-hepatocyte suspension (1×10^6 cells/ml) was incubated in Krebs-Henseleit buffer without serum in the presence of 10 μM of the test drug at 37°C under an atmosphere of 5% CO_2/95% O_2. The final concentration of acetonitrile was 0.5% (v/v) in the reaction mixture. The plates (24 wells) were shaken gently with an orbital shaker. The incubation mixture was sampled at 0, 0.25, 0.5, 1, and 2 h after treatment, and reactions were stopped by freezing the mixture in liquid nitrogen. When required, the samples were thawed, spiked with two volumes of acetonitrile or methanol containing an internal standard, and centrifuged. Aliquots of the supernatants were subjected to LC/MS/MS.

LC/MS/MS Conditions. Aliquots (10 μl) of plasma and h-hepatocyte suspension were introduced into the high-performance liquid chromatography system with an autosampler (Agilent Technologies, Santa Clara, CA). Several mobile phase conditions were used. Mobile phase condition 1 consisted of 10 mM ammonium acetate (A) and acetonitrile (B) on an Inertsil ODS-3 column (3 μm, 50 × 2.1 mm; GL Sciences Inc., Tokyo, Japan) at 40°C for the analysis of diclofenac, ibuprofen, ketoprofen, mirtazapine, (*S*)-naproxen, sulindac, and (*S*)-warfarin. The flow rate was set at 0.2 ml/min. The starting condition for the high-performance liquid chromatography gradient was 90:10 (A/B). From 0 to 5 min, the mobile phase composition was changed linearly to 10:90 (A/B), and this was held until 8 min. The gradient then was returned to 90:10 (A/B)

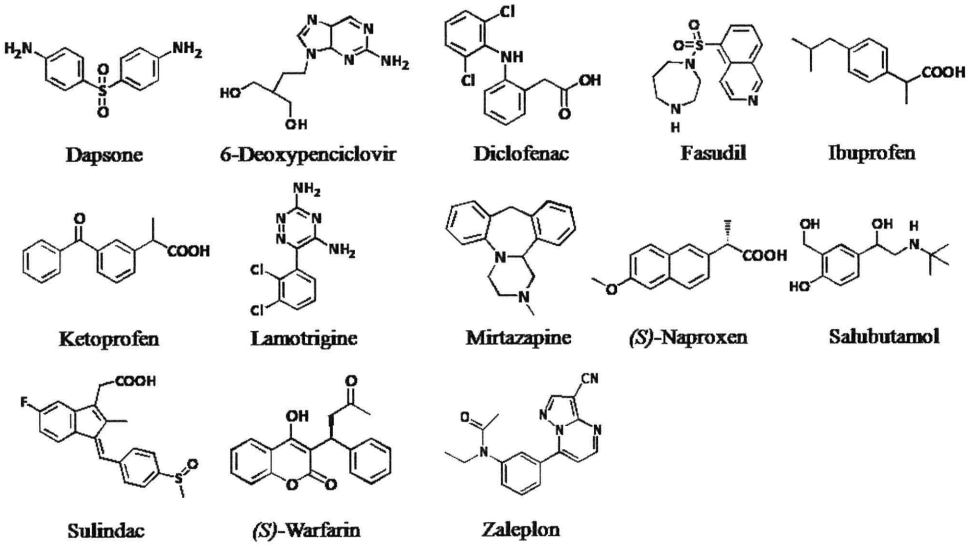

FIG. 1. Chemical structures of the model compounds used in this study.

TABLE 1

Literature values of plasma clearance, half-life, unbound fraction in plasma, blood/plasma concentration ratio, and metabolic enzymes in humans for the model compounds examined in this analysis

Rb values of fasudil, lamotrigine, and sulindac were assumed to be 1 due to unavailable data from the literature. References are in Supplemental Tables 1 and 2.

Compounds	CL_t or CL_{oral}	$t_{1/2}$	fu	Rb	Metabolic Enzymes
	$ml \cdot min^{-1} \cdot kg^{-1}$	*h*			
Dapsone	0.48	22	0.25	1.04	CYP2C9, CYP3A4, NAT
6-Deoxypenciclovir*,†	118	–	1	1.2	AO
Diclofenac	3.5	1.4	0.005	0.55	CYP2C9, UGT2B7, UGT1A9
Fasudil	73.2	0.26	0.51	1	AO
Ibuprofen	0.82	1.6	0.006	0.55	CYP2C9, UGT2B7
Ketoprofen	1.6	2.1	0.008	0.55	UGT2B7
Lamotrigine*	0.3	–	0.45	1	UGT1A4, UGT2B7
Mirtazapine	8.0	15	0.15	0.67	CYP1A2, CYP2D6, CYP3A4
(*S*)-Naproxen	0.1	–	0.01	0.55	CYP2C9, CYP1A2, UGT2B7
Salbutamol	7.7	3.9	0.925	0.96	SULT1A3
Sulindac*	3.3	–	0.069	1	AO
(*S*)-Warfarin	0.055	29	0.015	0.55	CYP2C9
Zaleplon	16	1.1	0.4	0.99	AO, CYP3A4

* From oral administration data.
† Calculated as famciclovir, which is prodrug of 6-deoxypenciclovir.
–, Unavailable data from intravenous administration.

linearly from 8 to 8.1 min, and the column was re-equilibrated to the initial condition.

Mobile phase condition 2 consisted of 0.1% formic acid (A) and methanol (B) on a YMC-Triart C18 column (3 μm, 50 × 2.1 mm; YMC Co., Ltd., Kyoto, Japan) for the analysis of dapsone, 6-deoxypenciclovir, fasudil, lamotrigine, salbutamol, and zaleplon. The starting condition was 90:10 (A/B). From 0 to 5 min, the mobile phase composition was changed linearly to 10:90 (A/B), and this was maintained until 8 min, then the column was re-equilibrated to the initial condition.

The MS/MS experiments were conducted by using API2000 LC/MS/MS systems (Applied Biosystems, Foster, CA). Mass number of the ionization mode, molecular ion, and product ion for the model compounds were as follows: dapsone m/z = 248.99 $[M + H]^+$ to 92.18, 6-deoxypenciclovir m/z = 238.05 $[M + H]^+$ to 210.95, diclofenac m/z = 294.14 $[M + H]^-$ to 249.53, fasudil m/z = 292.07 $[M + H]^+$ to 99.09, ibuprofen m/z = 204.88 $[M + H]^-$ to 158.52, ketoprofen m/z = 253.16 $[M + H]^-$ to 208.73, lamotrigine m/z = 256.03 $[M + H]^+$ to 210.96 mirtazapine m/z = 266.14 $[M + H]^+$ to 194.97, (*S*)-naproxen m/z = 228.68 $[M + H]^-$ to 168.55, salbutamol m/z = 240.18 $[M + H]^+$ to148.03, sulindac m/z = 357.07 $[M + H]^+$ to 232.96, (*S*)-warfarin m/z = 309.06 $[M + H]^+$ to162.97, zaleplon m/z = 306.08 $[M + H]^+$ to 236.12.

Determination of PK Parameters. Pharmacokinetic parameters were determined by noncompartmental methods using the concentration-time curve profile. The total clearances (CL_t) after intravenous administration were calculated as dose/AUC_{iv}. AUC_{iv} values were estimated from the time course using the trapezoidal method with extrapolation from the last quantifiable point to infinity. The terminal elimination $t_{1/2}$ was estimated as ln 2/*ke*, where *ke* is that of the plot of the terminal elimination phase on a logarithmic scale.

Calculation of In Vitro Intrinsic Clearance. In vitro intrinsic clearance ($CL_{int,in\ vitro}$) was calculated from the time course of the disappearance of the test drug during incubation with h-hepatocytes. Each plot was fitted to the first-order elimination rate constant as $C(t) = C_0 * \exp(-ke * t)$, where $C(t)$ and C_0 are the concentration of unchanged test drug at incubation time t and that at preincubation and *ke* is the disappearance rate constant of the unchanged drug.

Subsequently, $CL_{int,in\ vitro}$ ($\mu l \cdot min^{-1} \cdot 10^6\ cells^{-1}$) values were converted to $CL_{int,in\ vitro}$ ($ml \cdot min^{-1} \cdot kg^{-1}$) for the whole body. $CL_{int,in\ vitro}$ data were scaled up using physiological parameters, human liver weight 26 g/kg (Davies and Morris, 1993) and PXB mouse liver weight 140 g/kg, and the hepatocellularity (132 × 10^6 cells/g liver) of PXB mice. These parameters were taken from the average of observed data in PXB mice (RI = 80%).

Calculation of In Vivo Intrinsic Clearance. CL_t of PXB mice was calculated from the plasma concentrations after dosing using noncompartmental methods as described. CL_t was assumed to be equal to the hepatic clearance.

Values of CL_t, plasma unbound fraction (fu), and blood/plasma concentration ratio (Rb) in humans were taken from the literature.

In vivo intrinsic clearance ($CL_{int,in\ vivo}$) was calculated from the in vivo CL_t, fu, Rb, and average hepatic blood flow (Q) based on a well stirred model as $CL_{int,in\ vivo} = CL_t/\{(fu/Rb) \times (1 - CL_t/Q)\}$ (Pang and Rowland, 1977). These CL_t values were converted to blood clearance using Rb values.

The Q values of humans and PXB mice were set at 21 and 90 $ml \cdot min^{-1} \cdot kg^{-1}$ (same as in normal mice), respectively (Davies and Morris, 1993). In addition, Rb and fu of human were assumed to be equivalent to those of PXB mice. If CL_t of drugs exceeded liver blood flow, then the hepatic clearance was taken as 90% of liver blood flow. $CL_{int,in\ vivo}$ of 6-deoxypenciclovir, lamotrigine, and sulindac were evaluated from oral clearance (CL_{oral}) as CL_{oral}/fu/Rb.

Results

Selection of the Model Compounds for Analysis. In this study, we selected 13 compounds with diverse chemical structures (Fig. 1); Elimination of these selected drugs involves multiple metabolic pathways mediated not only by P450 but also by non-P450 enzymes, such as UGT, SULT, and aldehyde oxidase (AO) in liver. Mirtazapine and warfarin were known to be mainly metabolized by P450. Diclofenac, ibuprofen, and naproxen were metabolized by both UGT and P450. Furthermore, the model compounds metabolized by AO, such as

TABLE 2

Estimation of $CL_{int,in\ vitro}$ ($\mu l \cdot min^{-1} \cdot 10^6\ cells^{-1}$) in PXB mice hepatocytes and scaling to humans and PXB mice

$CL_{int,in\ vitro}$ ($\mu l \cdot min^{-1} \cdot 10^6\ cells^{-1}$) values were converted to $CL_{int,in\ vitro}$ ($ml \cdot min^{-1} \cdot kg^{-1}$) for the whole body. $CL_{int,in\ vitro}$ data were scaled up using physiological parameters, human liver weight (26 g/kg) and PXB mouse liver weight (140 g/kg), and the hepatocellularity (132 × 10^6 cells/g liver) of PXB mice. Each value represents the mean ± S.D. (n = 3).

Compounds	$CL_{int,in\ vitro}$	Scaled $CL_{int,in\ vitro}$ (Human)	Scaled $CL_{int,in\ vitro}$ (PXB Mice)
	$\mu l \cdot min^{-1} \cdot 10^6\ cells^{-1}$	$ml \cdot min^{-1} \cdot kg^{-1}$	
Dapsone	2.3 ± 1.2	8.0 ± 4.0	43.1 ± 21.3
6-Deoxypenciclovir	5.3 ± 1.2	18.3 ± 4.2	98.6 ± 22.4
Diclofenac	24.7 ± 1.2	84.7 ± 4.0	455.8 ± 21.3
Fasudil	35.7 ± 13.3	122.4 ± 45.6	659.1 ± 245.4
Ibuprofen	13.3 ± 2.1	45.8 ± 7.1	246.4 ± 38.5
Ketoprofen	6.0 ± 1.0	20.6 ± 3.4	110.9 ± 18.5
Lamotrigine	1.4 ± 1.0	4.8 ± 3.6	25.9 ± 19.2
Mirtazapine	6.3 ± 1.2	21.7 ± 4.0	117.0 ± 21.3
(*S*)-Naproxen	12.7 ± 2.5	43.5 ± 8.6	234.1 ± 46.5
Salbutamol	1.0 ± 1.0	3.3 ± 3.3	17.9 ± 17.8
Sulindac	2.0 ± 2.0	7.0 ± 6.7	37.6 ± 36.0
(*S*)-Warfarin	1.2 ± 0.7	4.1 ± 2.5	22.2 ± 13.3
Zaleplon	2.3 ± 1.2	8.0 ± 4.0	43.1 ± 21.3

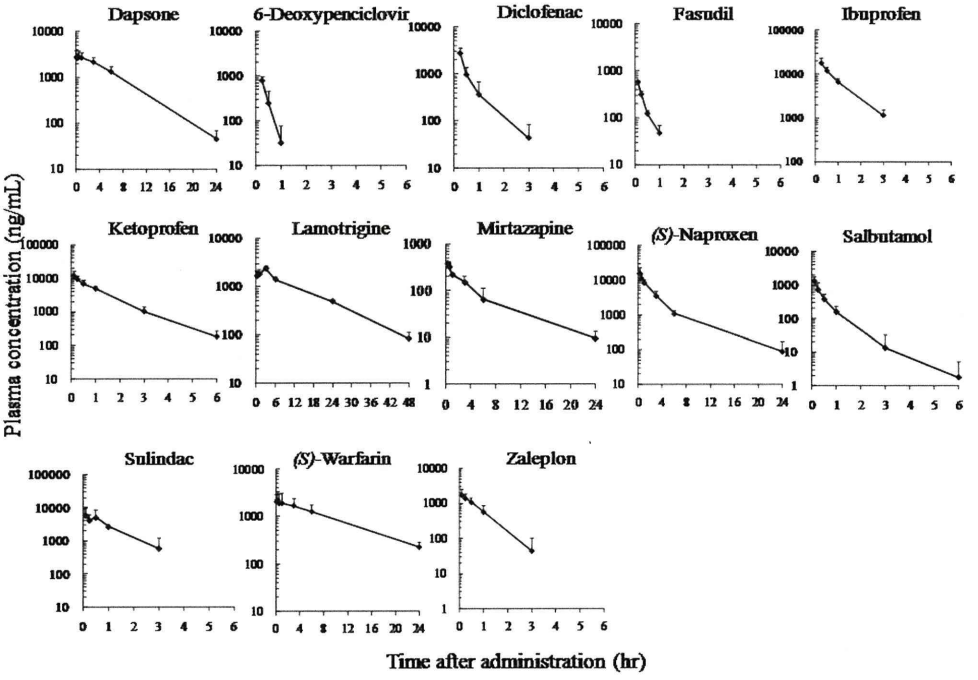

FIG. 2. Plasma concentrations after intravenous administration to PXB mice. Each point represents the mean ± S.D. (n = 3–5).

6-deoxypenciclovir, fasudil, sulindac, and zaleplon, were added in this study. These were reflected in the data set that spanned a wide range of PK parameter characteristics. CL_t and $t_{1/2}$ after intravenous administration of selected model drugs to humans were obtained from the literature. If CL_t after intravenous administration was not available from the literature, we used the value of CL_t/F after oral administration. The PK parameters and the major enzymes responsible for drug metabolism in humans are shown in Table 1. The spreadsheet containing these values with the literature references is included as an attachment in the supplemental data (Supplemental Tables 1 and 2).

Disappearance of Parent Drugs after Incubation. Remaining amounts of all of the compounds decreased linearly for 2 h on incubation with h-hepatocytes. The values of $CL_{int,in\ vitro}$ in hepatocytes, calculated using scaling factors to humans and PXB mice whole body as described under *Materials and Methods*, are listed in Table 2. These $CL_{int,in\ vitro}$ values covered a wide range. Fasudil showed high clearance, whereas warfarin was very stable.

PK Study of the Model Compounds in PXB Mice. Plasma concentrations and PK parameters in PXB mice after intravenous administration of drug solutions at 0.3 to 5 mg/kg are shown in Fig. 2 and Tables 3 and 4. Each RI value in PXB mice was 73.4 to 93.4%.

CL_t values of warfarin and lamotrigine were relatively low, whereas those of fasudil and salbutamol were much higher; the range of CL_t was 0.2 to 198 ml · min^{-1} · kg^{-1}. The $t_{1/2}$ value of lamotrigine was the longest, and those of 6-deoxypenciclovir and fasudil were short, as shown in Table 3.

Comparison of Intrinsic CL between h-Hepatocytes and Humans. Direct comparison between $CL_{int,in\ vitro}$ from h-hepatocytes and $CL_{int,in\ vivo}$ calculated for a well stirred model in humans showed a moderate correlation (r^2 = 0.475, p = 0.009) (Fig. 3). For 2 of 13 (15%) compounds, observed $CL_{int,in\ vivo}$ was predicted within a 3-fold error from hepatocyte $CL_{int,\ in\ vitro}$. However, for 8 of 13 (62%) compounds, observed $CL_{int,in\ vivo}$ was predicted with a 3- to 10-fold error.

Figure 4 shows the relationship between $CL_{int,in\ vivo}$ and $CL_{int,in\ vitro}$ for PXB mice; again, the correlation was moderate (r^2 = 0.435, p =

TABLE 3

Experimental conditions and RI values in PXB mice used for PK study

Each compound was administered intravenously to PXB mice at 0.3 to 5 mg/kg body weight. The values of RI of PXB mice ranged from 73.4 to 93.4%. Each value represents the mean ± S.D. (n = 3–5).

Compounds	Dose	RI	CL_t	$t_{1/2}$
	mg/kg	*%*	*ml · min^{-1} · kg^{-1}*	*h*
Dapsone	3.0	77.4 ± 5.5	2.1 ± 0.5	4.5 ± 1.1
6-Deoxypenciclovir	3.0	93.4 ± 4.2	71.2 ± 13.0	0.1 ± 0.1
Diclofenac	3.0	76.4 ± 2.1	16.4 ± 4.3	0.6 ± 0.2
Fasudil	3.0	75.8 ± 1.3	198.1 ± 14.6	0.3 ± 0.1
Ibuprofen	5.0	73.4 ± 3.2	3.8 ± 1.0	0.7 ± 0.1
Ketoprofen	3.0	74.0 ± 1.1	3.3 ± 0.6	1.1 ± 0.1
Lamotrigine	3.0	77.1 ± 4.0	1.4 ± 0.2	10.1 ± 0.9
Mirtazapine	3.0	79.8 ± 1.7	30.4 ± 9.4	6.0 ± 1.4
(*S*)-Naproxen	5.0	82.2 ± 6.1	2.2 ± 0.5	4.8 ± 2.7
Salbutamol	3.0	74.5 ± 0.7	79.9 ± 34.0	0.6 ± 0.3
Sulindac	3.0	74.5 ± 2.0	5.6 ± 1.3	1.2 ± 0.8
(*S*)-Warfarin	0.3	75.3 ± 1.8	0.2 ± 0.1	8.2 ± 2.8
Zaleplon	3.0	77.1 ± 3.7	48.1 ± 7.1	0.7 ± 0.4

TABLE 4

$CL_{int,in\ vivo}$ of humans and PXB mice, calculated by a well stirred model

$CL_{int,in\ vivo}$ was calculated from in vivo CL_t, fu, Rb, and Q based on a well stirred model. The Q values of humans and PXB mice were set at 21 and 90 ml · min^{-1} · kg^{-1} (same as in normal mice), respectively. In addition, Rb and fu of human were assumed to be equivalent to those of PXB mice. If total CL of drugs exceeded liver blood flow, then the hepatic clearance was taken as 90% of liver blood flow. $CL_{int,in\ vivo}$ of 6-deoxypenciclovir, lamotrigine, and sulindac were evaluated from CL_{oral} as CL_{oral}/fu/Rb.

Compounds	Human $CL_{int,in\ vivo}$	PXB Mice $CL_{int,in\ vivo}$
	ml · min^{-1} · kg^{-1}	
Dapsone	2.0	8.6
6-Deoxypenciclovir	118.0	209.0
Diclofenac	1004.3	4905.1
Fasudil	370.6	1588.2
Ibuprofen	147.1	686.0
Ketoprofen	232.2	442.0
Lamotrigine	0.7	3.2
Mirtazapine	123.6	408.7
(*S*)-Naproxen	10.1	230.2
Salbutamol	13.5	1148.2
Sulindac	47.8	86.5
(*S*)-Warfarin	3.7	13.4
Zaleplon	173.6	261.3

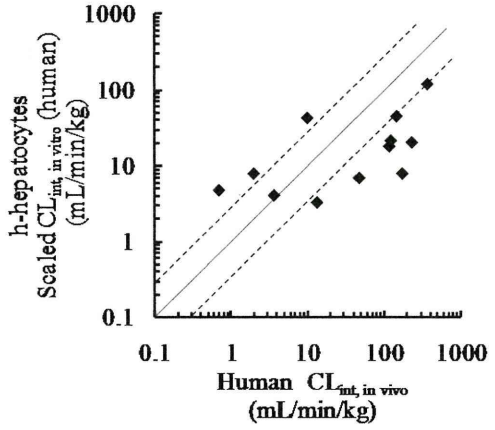

FIG. 3. Correlation between observed human $CL_{int,in\ vivo}$ and $CL_{int,in\ vitro}$ of PXB mouse hepatocytes, calculated as described in the text. The solid line represents unity. The dotted line represents the range within 3-fold of unity.

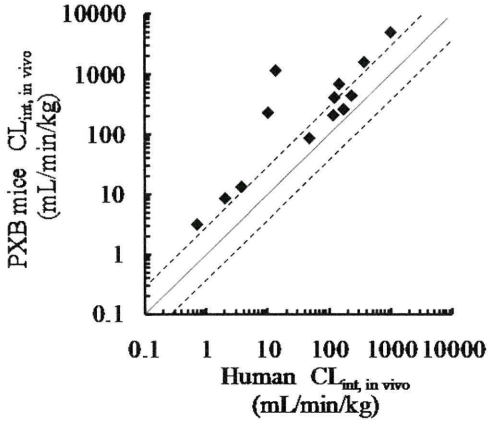

FIG. 5. Correlation of $CL_{int,in\ vivo}$ between humans and PXB mice, calculated as described in the text. The solid line represents unity. The dotted line represents the range within 3-fold of unity.

0.014). For 6 of 13 (46%) compounds, $CL_{int,in\ vivo}$ of PXB mice was predicted within a 3-fold error from h-hepatocyte $CL_{int,in\ vitro}$. For 5 of 13 (38%) compounds, $CL_{int,in\ vivo}$ was predicted within a 3- to 10-fold error.

Relationship between Intrinsic Clearance in Humans and PXB Mice In Vivo. We directly compared $CL_{int,in\ vivo}$ calculated based on a well stirred model in humans and PXB mice. As shown in Fig. 5, there was a good correlation ($r^2 = 0.754$, $p = 1.174 \times 10^{-4}$) between literature $CL_{int,in\ vivo}$ in human and measured $CL_{int,in\ vivo}$ of PXB mice for these compounds. For 4 of 13 (31%) compounds, observed $CL_{int\ in\ vivo}$ in humans was predicted within a 3-fold error from PXB mouse $CL_{int,in\ vivo}$. For 7 of 13 (54%) compounds, human $CL_{int,in\ vivo}$ was predicted within a 3- to 10-fold error.

Relationship of Elimination $t_{1/2}$ between Humans and PXB mice. Figure 6 shows the relationship of $t_{1/2}$ after intravenous administration between humans and PXB mice. Compounds for which literature data were not available were excluded from this figure. A good correlation ($r^2 = 0.886$, $p = 1.506 \times 10^{-4}$) was found. For 6 of 9 (67%) compounds, human observed $t_{1/2}$ was predicted within a 3-fold error from PXB mice $t_{1/2}$. For 3 of 9 (33%) compounds, the error was in the range of 3- to 10-fold.

Discussion

The prediction of human PK parameters is an important step during the preclinical development of pharmaceuticals to reduce costs by enabling the early elimination of candidates with unsuitable properties. However, species differences make it difficult to predict human PK from animal data; monkey data may lead to underprediction (Chiou and Buehler, 2002; Akabane et al., 2010), whereas dog data may cause overestimation (Chiou et al., 2000). In vitro-in vivo scaling from data obtained with human hepatic microsomes and hepatocytes is a widely used approach but often results in the underprediction of in vivo CL (Obach, 1999). We considered the possibility that PXB mice, in which hepatocytes are replaced with human hepatocytes to the extent of approximately 80% (Tateno et al., 2004), may have superior predictive utility, because the expression levels and activities of both P450 and non-P450 enzymes well reflect those of the donor hepatocytes (Yoshitsugu et al., 2006; Yamasaki et al., 2010). In this study, we checked metabolic activities (CYP2C9, CYP2D6, UGT, SULT, and AO) using probe substrates between donor hepatocytes and h-hepatocytes purified from PXB mice (Supplemental Table 3) as well as the expression of drug transporters and blood albumin (Tateno et al., 2004; Nishimura et al., 2005).

For the present study, we selected 13 model compounds with diverse chemical structures (Fig. 1), which are metabolized through multiple pathways by P450 and non-P450 enzymes, such as UGT, SULT, and AO. Their values of CL cover a wide range from 0.055 to 118 $ml \cdot min^{-1} \cdot kg^{-1}$ (Table 1).

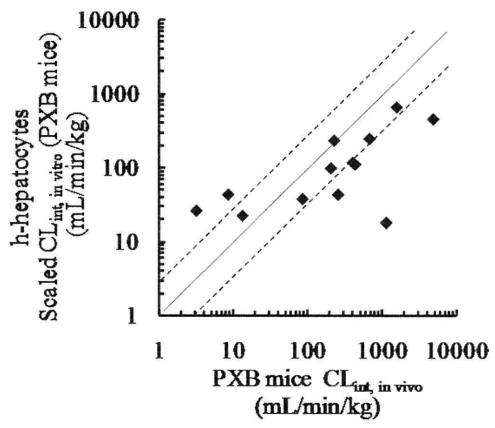

FIG. 4. Correlation between $CL_{int,in\ vivo}$ of PXB mice and $CL_{int,in\ vitro}$ of their hepatocytes, calculated as described in the text. The solid line represents unity. The dotted line represents the range within 3-fold of unity.

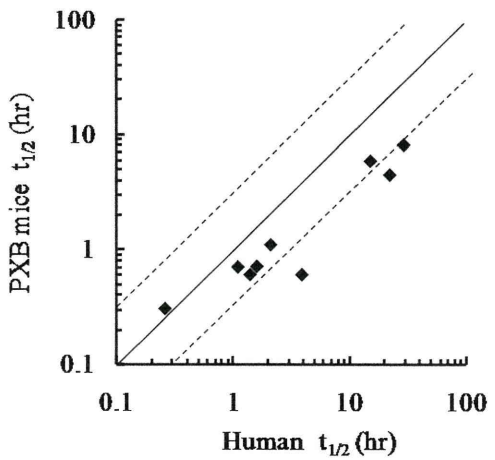

FIG. 6. Correlation of $t_{1/2}$ after intravenous administration between humans and PXB mice. Compounds for which literature data were not available were excluded from this figure. The solid line represents unity. The dotted line represents the range within 3-fold of unity.

First, we performed an in vitro metabolic study using fresh h-hepatocytes isolated from PXB mice. We calculated $CL_{int,in\ vitro}$ using fresh h-hepatocytes and compared the results with human $CL_{int,in\ vivo}$ estimated by use of a well stirred model (Pang and Rowland, 1977). These results using a parallel tube model and a dispersion model were also similar to those of a well stirred model (S. Sanoh, unpublished observations). A moderate correlation ($r^2 = 0.475$, $p = 0.009$) was found, but this approach was not superior to prediction using other methods.

$CL_{int,in\ vitro}$ values of diclofenac, ibuprofen, warfarin, and zaleplon were approximately similar to reported values using cryopreserved hepatocytes (Ekins and Obach, 2000; Nagilla et al., 2006; Stringer et al., 2008), supporting the idea that $CL_{int,in\ vitro}$ values are similar in fresh hepatocytes and cryopreserved hepatocytes (Naritomi et al., 2003; McGinnity et al., 2004).

A similar correlation ($r^2 = 0.435$, $p = 0.014$) was observed between $CL_{int,in\ vitro}$ and $CL_{int,in\ vivo}$ in PXB mice (Fig. 4). In both cases, the numbers of compounds for which absolute values of CL_{int} were predicted within a 3-fold error were insufficient.

Therefore, we next evaluated the predictability of hepatic clearance and $t_{1/2}$ from in vivo data in PXB mice. The values of $CL_{int,in\ vivo}$ estimated by intravenous administration in PXB mice were well correlated ($r^2 = 0.754$, $p = 1.174 \times 10^{-4}$) with observed $CL_{int,in\ vivo}$ in human. Surprisingly, we also found a good correlation ($r^2 = 0.886$, $p = 1.506 \times 10^{-4}$) between $t_{1/2}$ values in PXB mice and humans. However, although the rank order was the same, there were rather large prediction errors, so it may not be possible to predict absolute values. This is consistent with the findings of Xiao et al. (2010) in PXB mice.

We used PXB mice that showed that the average RI values were approximately 80%. It was a concern that the contribution of the remaining approximately 20% mice hepatocytes may be reflected on clearance. $CL_{int,in\ vitro}$ values of these model compounds in host mice hepatocytes (severe combined immunodeficiency mice) were almost higher than those of h-hepatocytes within a 10-fold range (Supplemental Fig. 1). The extent of the difference may not influence the predictability of $CL_{int,in\ vivo}$.

For the estimation of $CL_{int,in\ vivo}$ in PXB mice, the fu values of those model compounds is the same as those in humans because human albumin is expressed in the blood of PXB mice. Inoue et al. (2009) reported fu value of warfarin in PXB mice was similar to that in humans. Furthermore, fu values of some compounds (dapsone, diclofenac, ketoprofen, salbutamol, and zaleplon) in this study were also approximately similar to those in humans (S. Sanoh, unpublished observations).

We assumed that the Rb values of those model compounds is also the same as those in humans, because Rb values of some compounds (dapsone, diclofenac, ketoprofen, salbutamol, and zaleplon) in this study were also approximately similar to those in humans (S. Sanoh, unpublished observations).

Q values were assumed to be 90 ml $\cdot$ min^{-1} $\cdot$ kg^{-1}, respectively, corresponding to the values of normal mice (Davies and Morris, 1993). In further work, it would be desirable to examine whether these values are appropriate.

In this study, we selected model compounds metabolized not only by P450, but also by non-P450 enzymes, including AO. 6-Deoxypenciclovir, fasudil, sulindac, and zaleplon are metabolized mainly by AO in humans. It has been reported that human CL for drugs metabolized by AO may be underpredicted from data obtained with human liver cytosol and S9 due to the loss or deactivation of AO during preparation, homogenization, storage, and experimental procedures (Zientek et al., 2010). PXB mice have high AO activity, being similar to humans (Kitamura et al., 2008), and may be a useful source of fresh h-hepatocytes.

Our results indicate that PXB mice can be used at least for semi-quantitative prediction of not only CL_t but also $t_{1/2}$ in humans. PXB mice also would be useful for in vitro estimation and comparison of PK of various candidate compounds, because large amounts of fresh, identical hepatocytes (1.1×10^8 cells/mouse) are available by transplantation of donor hepatocytes (2.5×10^5 cells/mouse). The combination of in vitro study in PXB mice and in vitro study using PXB hepatocytes may prove to be particularly effective.

Acknowledgments

We thank members in PhoenixBio Co., Ltd. for the isolation of hepatocytes from PXB mice.

Authorship Contributions

Participated in research design: Sanoh, Sugihara, Kotake, Tayama, Horie, Kitamura, and Ohta.

Conducted experiments: Sanoh and Horiguchi.

Contributed new reagents or analytic tools: Sugihara, Ohshita, and Tateno.

Performed data analysis: Sanoh and Horiguchi.

Wrote or contributed to the writing of the manuscript: Sanoh, Kotake, Tateno, and Ohta.

References

Akabane T, Tabata K, Kadono K, Sakuda S, Terashita S, and Teramura T (2010) A comparison of pharmacokinetics between humans and monkeys. *Drug Metab Dispos* **38:**308–316.

Brown HS, Griffin M, and Houston JB (2007) Evaluation of cryopreserved human hepatocytes as an alternative in vitro system to microsomes for the prediction of metabolic clearance. *Drug Metab Dispos* **35:**293–301.

Chiba M, Ishii Y, and Sugiyama Y. (2009) Prediction of hepatic clearance in human from in vitro data for successful drug development. *AAPS J* **11:**262–276.

Chiou WL and Buehler PW (2002) Comparison of oral absorption and bioavailability of drugs between monkey and human. *Pharm Res* **19:**868–874.

Chiou WL, Jeong HY, Chung SM, and Wu TC (2000) Evaluation of using dog as an animal model to study the fraction of oral dose absorbed of 43 drugs in humans. *Pharm Res* **17:**135–140.

Davies B and Morris T (1993) Physiological parameters in laboratory animals and humans. *Pharm Res* **10:**1093–1095.

De Buck SS, Sinha VK, Fenu LA, Nijsen MJ, Mackie CE, and Gilissen RA (2007) Prediction of human pharmacokinetics using physiologically based modeling: a retrospective analysis of 26 clinically tested drugs. *Drug Metab Dispos* **35:**1766–1780.

De Serres M, Bowers G, Boyle G, Beaumont C, Castellino S, Sigafoos J, Dave M, Roberts A, Shah V, Olson K, et al. (2011) Evaluation of a chimeric (uPA+/+)/SCID mouse model with a humanized liver for prediction of human metabolism. *Xenobiotica* **41:**464–475.

Ekins S and Obach RS (2000) Three-dimensional quantitative structure activity relationship computational approaches for prediction of human in vitro intrinsic clearance. *J Pharmacol Exp Ther* **295:**463–473.

Fagerholm U (2007) Prediction of human pharmacokinetics–evaluation of methods for prediction of hepatic metabolic clearance. *J Pharm Pharmacol* **59:**803–828.

Hallifax D, Foster JA, and Houston JB (2010) Prediction of human metabolic clearance from in vitro systems: retrospective analysis and prospective view. *Pharm Res* **27:**2150–2161.

Huang L, Berry L, Ganga S, Janosky B, Chen A, Roberts J, Colletti AE, and Lin MH (2010) Relationship between passive permeability, efflux, and predictability of clearance from in vitro metabolic intrinsic clearance. *Drug Metab Dispos* **38:**223–231.

Inoue T, Sugihara K, Ohshita H, Horie T, Kitamura S, and Ohta S (2009) Prediction of human disposition toward S-3H-warfarin using chimeric mice with humanized liver. *Drug Metab Pharmacokinet* **24:**153–160.

Kamimura H, Nakada N, Suzuki K, Mera A, Souda K, Murakami Y, Tanaka K, Iwatsubo T, Kawamura A, and Usui T (2010) Assessment of chimeric mice with humanized liver as a tool for predicting circulating human metabolites. *Drug Metab Pharmacokinet* **25:**223–235.

Katoh M, Matsui T, Nakajima M, Tateno C, Kataoka M, Soeno Y, Horie T, Iwasaki K, Yoshizato K, and Yokoi T (2004) Expression of human cytochromes P450 in chimeric mice with humanized liver. *Drug Metab Dispos* **32:**1402–1410.

Katoh M, Matsui T, Okumura H, Nakajima M, Nishimura M, Naito S, Tateno C, Yoshizato K, and Yokoi T (2005) Expression of human phase II enzymes in chimeric mice with humanized liver. *Drug Metab Dispos* **33:**1333–1340.

Kitamura S, Nitta K, Tayama Y, Tanoue C, Sugihara K, Inoue T, Horie T, and Ohta S (2008) Aldehyde oxidase-catalyzed metabolism of N1-methylnicotinamide in vivo and in vitro in chimeric mice with humanized liver. *Drug Metab Dispos* **36:**1202–1205.

McGinnity DF, Soars MG, Urbanowicz RA, and Riley RJ (2004) Evaluation of fresh and cryopreserved hepatocytes as in vitro drug metabolism tools for the prediction of metabolic clearance. *Drug Metab Dispos* **32:**1247–1253.

Nagilla R, Frank KA, Jolivette LJ, and Ward KW (2006) Investigation of the utility of published in vitro intrinsic clearance data for prediction of in vivo clearance. *J Pharmacol Toxicol Methods* **53:**106–116.

Naritomi Y, Terashita S, Kagayama A, and Sugiyama Y (2003) Utility of hepatocytes in predicting drug metabolism: comparison of hepatic intrinsic clearance in rats and humans in vivo and in vitro. *Drug Metab Dispos* **31:**580–588.

Nishimura M, Yoshitsugu H, Yokoi T, Tateno C, Kataoka M, Horie T, Yoshizato K, and Naito

S (2005) Evaluation of mRNA expression of human drug-metabolizing enzymes and transporters in chimeric mouse with humanized liver. *Xenobiotica* **35:**877–890.

Obach RS (1999) Prediction of human clearance of twenty-nine drugs from hepatic microsomal intrinsic clearance data: An examination of in vitro half-life approach and nonspecific binding to microsomes. *Drug Metab Dispos* **27:**1350–1359.

Paixão P, Gouveia LF, and Morais JA (2010) Prediction of the in vitro intrinsic clearance determined in suspensions of human hepatocytes by using artificial neural networks. *Eur J Pharm Sci* **39:**310–321.

Pang KS and Rowland M (1977) Hepatic clearance of drugs. I. Theoretical considerations of a "well-stirred" model and a "parallel tube" model. Influence of hepatic blood flow, plasma and blood cell binding, and the hepatocellular enzymatic activity on hepatic drug clearance. *J Pharmacokinet Biopharm* **5:**625–653.

Stringer R, Nicklin PL, and Houston JB (2008) Reliability of human cryopreserved hepatocytes and liver microsomes as in vitro systems to predict metabolic clearance. *Xenobiotica* **38:**1313–1329.

Tabata K, Hamakawa N, Sanoh S, Terashita S, and Teramura T (2009) Exploratory population pharmacokinetics (e-PPK) analysis for predicting human PK using exploratory ADME data during early drug discovery research. *Eur J Drug Metab Pharmacokinet* **34:**117–128.

Tateno C, Yoshizane Y, Saito N, Kataoka M, Utoh R, Yamasaki C, Tachibana A, Soeno Y, Asahina K, Hino H, et al. (2004) Near completely humanized liver in mice shows human-type metabolic responses to drugs. *Am J Pathol* **165:**901–912.

Wang Q, Jia R, Ye C, Garcia M, Li J, and Hidalgo IJ (2005) Glucuronidation and sulfation of 7-hydroxycoumarin in liver matrices from human, dog, monkey, rat, and mouse. *In Vitro Cell Dev Biol Anim* **41:**97–103.

Xiao G, Bohnert T, Black C, Klunk L, and Gan LS (2010) Evaluation of chimeric mice with humanized liver to predict human intrinsic clearance of drug molecules at preclinical phase. *Drug Metab Rev* **42(S1:)**P60.

Yamasaki C, Kataoka M, Kato Y, Kakuni M, Usuda S, Ohzone Y, Matsuda S, Adachi Y, Ninomiya S, Itamoto T, et al. (2010) In vitro evaluation of cytochrome P450 and glucuronidation activities in hepatocytes isolated from liver-humanized mice. *Drug Metab Pharmacokinet* **25:**539–550.

Yamazaki H, Kuribayashi S, Inoue T, Tateno C, Nishikura Y, Oofusa K, Harada D, Naito S, Horie T, and Ohta S (2010) Approach for in vivo protein binding of 5-n-butyl-pyrazolo[1,5-a]pyrimidine bioactivated in chimeric mice with humanized liver by two-dimensional electrophoresis with accelerator mass spectrometry. *Chem Res Toxicol* **23:**152–158.

Yoshitsugu H, Nishimura M, Tateno C, Kataoka M, Takahashi E, Soeno Y, Yoshizato K, Yokoi T, and Naito S (2006) Evaluation of human CYP1A2 and CYP3A4 mRNA expression in hepatocytes from chimeric mice with humanized liver. *Drug Metab Pharmacokinet* **21:**465–474.

Zientek M, Jiang Y, Youdim K, and Obach RS (2010) In vitro-in vivo correlation for intrinsic clearance for drugs metabolized by human aldehyde oxidase. *Drug Metab Dispos* **38:**1322–1327.

Address correspondence to: Dr. Seigo Sanoh, Graduate School of Biomedical Sciences, Hiroshima University, Kasumi 1-2-3, Minami-ku, Hiroshima 734-8553 Japan. E-mail: sanoh@hiroshima-u.ac.jp

1521-009X/12/4003-474–480$25.00
DRUG METABOLISM AND DISPOSITION
Vol. 40, No. 3
42754/3748075

DMD 40:474–480, 2012

Investigation of Drug-Drug Interactions Caused by Human Pregnane X Receptor-Mediated Induction of CYP3A4 and CYP2C Subfamilies in Chimeric Mice with a Humanized Liver[S]

Maki Hasegawa, Harunobu Tahara, Ryo Inoue, Masakazu Kakuni, Chise Tateno, and Junko Ushiki

Kyowa Hakko Kirin Co., Ltd., Nagaizumi-cho, Sunto-gun, Shizuoka, Japan (M.H., H.T., J.U.); and PhoenixBio, Co., Ltd., Higashihiroshima-shi, Hiroshima, Japan (R.I., M.K., C.T.)

Received September 14, 2011; accepted November 29, 2011

ABSTRACT:

The induction of cytochrome P450 (P450) enzymes is one of the risk factors for drug-drug interactions (DDIs). To date, the human pregnane X receptor (PXR)-mediated CYP3A4 induction has been well studied. In addition to CYP3A4, the expression of CYP2C subfamily is also regulated by PXR, and the DDIs caused by the induction of CYP2C enzymes have been reported to have a major clinical impact. The purpose of the present study was to investigate whether chimeric mice with a humanized liver (PXB mice) can be a suitable animal model for investigating the PXR-mediated induction of CYP2C subfamily, together with CYP3A4. We evaluated the inductive effect of rifampicin (RIF), a typical human PXR ligand, on the plasma exposure to the four P450 substrate drugs (triazolam/CYP3A4, pioglitazone/CYP2C8, (*S*)-warfarin/CYP2C9, and (*S*)-(−)-mephenytoin/CYP2C19) by cassette dosing in PXB mice. The induction of several drug-metabolizing enzymes and transporters in the liver was also examined by measuring the enzyme activity and mRNA expression levels. Significant reductions in the exposure to triazolam, pioglitazone, and (*S*)-(−)-mephenytoin, but not to (*S*)-warfarin, were observed. In contrast to the in vivo results, all the four P450 isoforms, including CYP2C9, were elevated by RIF treatment. The discrepancy in the (*S*)-warfarin results between in vivo and in vitro studies may be attributed to the relatively small contribution of CYP2C9 to (*S*)-warfarin elimination in the PXB mice used in this study. In summary, PXB mice are a useful animal model to examine DDIs caused by PXR-mediated induction of CYP2C and CYP3A4.

Introduction

The induction of cytochrome P450 (P450) enzymes is one of the risk factors for drug-drug interactions (DDIs) (Niemi et al., 2003; Luo et al., 2004). The human pregnane X receptor (PXR) is a key nuclear receptor principally responsible for the induction of several P450 enzymes, including CYP3A4, -2C8, -2C9, -2C19, -2A6, and -2B6 (Niemi et al., 2003; Sinz et al., 2008; Chen and Goldstein, 2009). In addition to P450 enzymes, the expression of several drug transporters, such as multidrug resistance gene (MDR) 1, multidrug resistance-associated protein (MRP) 2, organic anion-transporting polypeptides, and phase II metabolic enzymes, including UDP-glucuronosyltransferase (UGT), sulfotransferase, and glutathione S-transferase, are also regulated by human PXR (Dixit et al., 2007; Nishimura et al., 2008a,b; Sinz et al., 2008).

In humans, CYP3A4 plays a major role in drug metabolism because of its abundant expression in the liver and intestine and its broad substrate specificity. In fact, CYP3A4 contributes to the oxidative metabolism of more than 50% of all currently used drugs (de Wildt et al., 1999; Luo et al., 2004). Therefore, CYP3A4-related DDIs have a major clinical impact. CYP3A4 is the most studied isoform among the P450s in terms of DDIs caused by PXR-related induction of drug-metabolizing enzymes. Both in vitro and in vivo experimental models for CYP3A4 induction have been reported by several pharmaceutical companies (Cui et al., 2008; Kanebratt and Andersson, 2008; Kim et al., 2008, 2010; Kamiguchi et al., 2010).

The human CYP2C subfamily has four members: CYP2C8, CYP2C9, CYP2C18, and CYP2C19 (Läpple et al., 2003; Chen and Goldstein, 2009). Of these, CYP2C8, CYP2C9, and CYP2C19 are of clinical importance and are collectively responsible for the metabolism of ~20% of clinically used drugs (Chen and Goldstein, 2009). The substrate specificity of CYP3A4 and CYP2C enzymes sometimes overlaps. In that case, the overall contribution of PXR-regulated P450 enzymes in the drug elimination process is relatively large. These observations suggest that new investigations should focus on the DDIs

Article, publication date, and citation information can be found at http://dmd.aspetjournals.org.
http://dx.doi.org/10.1124/dmd.111.042754.
[S] The online version of this article (available at http://dmd.aspetjournals.org) contains supplemental material.

ABBREVIATIONS: P450, cytochrome P450; DDI, drug-drug interaction; PXR, pregnane X receptor; MDR, multidrug resistance gene; MRP, multidrug resistance-associated protein; UGT, UDP-glucuronosyltransferase; RIF, rifampicin; ROS, rosiglitazone; WAR, (*S*)-warfarin; MEP, (*S*)-(−)-mephenytoin; TRZ, triazolam; GAPDH, glyceraldehyde-3-phosphate dehydrogenase; PCR, polymerase chain reaction; G-6-P, D-glucose 6-phosphate; G-6-P-DH, G-6-P dehydrogenase; LC/MS/MS, liquid chromatography-tandem mass spectrometry; AUC, area under the plasma concentration-time curve.

between PXR ligands and CYP2C substrate drugs. The quantitative polymerase chain reaction (PCR) analyses using human hepatocytes have demonstrated that the magnitude of CYP3A4 induction by PXR ligand is the largest followed by CYP2C enzymes, including CYP2C8, CYP2C9, and CYP2C19 (Raucy et al., 2002; Niemi et al., 2003). In fact, DDIs caused by induction of CYP2C enzymes have been also reported (Chen and Goldstein, 2009). However, there has been no systematic in vivo analysis focusing on the differences in the degree of the inductive effects of PXR ligands on the each of these P450 enzymes.

It has been reported that there is a large species difference in ligand recognition by the PXR between rodents and humans (Jones et al., 2000; LeCluyse, 2001). For example, RIF is more selective for human PXR, whereas the synthetic C21 steroid pregnenolone-16[propto]-carbonitrile, is a weak ligand for the human PXR but a potent ligand for rodents (Jones et al., 2000; LeCluyse, 2001). In fact, the expression of mouse Cyp3a is not influenced by the administration of RIF (Ma et al., 2007). The species differences in the ligand recognition of the PXR limit the utility of animal models to predict PXR-related DDIs in humans. In addition, it is known that there are species differences in metabolic patterns, as well as in the contribution of each P450 isoform to drug elimination (Shin et al., 2009; Kamimura et al., 2010). These species differences make it hard to predict human pharmacokinetics from animal data. Recently, several groups, including our own, have generated the humanized mouse models of the PXR and CYP3A4 by gene knockout and transgenic techniques (Xie et al., 2000; Ma et al., 2007; Kim et al., 2008; Scheer et al., 2008; Hasegawa et al., 2011). These models are useful for investigating CYP3A4 induction by human PXR ligands. However, the effect of the human PXR ligand on drug-metabolizing enzymes other than CYP3A4 cannot be examined using these mouse models.

The chimeric mouse with a humanized liver is an alternative mouse model (Strom et al., 2010). This mouse model, designated as the "PXB mouse," has been established by the transplantation of human hepatocytes into urokinase-type plasminogen activator-transgenic severe combined immunodeficient mice (Tateno et al., 2004). The livers of the PXB mice are replaced with more than 70% human hepatocytes, although the remaining 30% are mouse hepatocytes (Strom et al., 2010). It has been reported that the mRNA expression of several P450 enzymes in the PXB mouse liver is induced by RIF treatment and that PXB mice also show similar drug-metabolizing profiles of CYP3A4 and CYP2C substrate drugs to humans (Katoh et al., 2005a,b; Kamimura et al., 2010). The PXB mouse is expected to provide the opportunity to examine the inductive effect of PXR ligands on the plasma profiles of not only CYP3A4 but also CYP2C substrate drugs. This study will provide important information on DDIs caused by CYP2C induction in addition to CYP3A4.

In the present study, we evaluated the inductive effect of three different doses of RIF on the plasma exposure of PXB mice to the substrate drugs of CYP3A4, CYP2C8, CYP2C9, and CYP2C19, which have been reported to have DDIs with RIF in humans. Furthermore, the induction of several drug-metabolizing enzymes and transporters in the liver was also examined by measuring the enzyme activities and mRNA expression levels.

Materials and Methods

Materials. RIF, rosiglitazone (ROS), (*S*)-warfarin (WAR), dextromethorphan hydrobromide monohydrate, and propranolol hydrochloride were purchased from Wako Pure Chemical Industries (Osaka, Japan). Triazolam (TRZ), phenacetin, bupropion, and diclofenac were purchased from Sigma-Aldrich (St. Louis, MO). (*S*)-(−)-Mephenytoin (MEP) was purchased from Toronto Research Chemicals (North York, Canada). $NADP^+$, D-glucose 6-phosphate (G-6-P), and G-6-P dehydrogenase (G-6-P-DH) were purchased from Oriental Yeast (Tokyo, Japan). All other chemicals and solvents were of analytical grade otherwise noted.

Generation of Chimeric Mice with a Humanized Liver. All animal studies were conducted in accordance with the *Guiding Principles for the Care and Use of Laboratory Animals*, and the experimental protocol used in this study was approved by the Committee for Animal Experiments of PhoenixBio Co., Ltd., and Kyowa Hakko Kirin Co., Ltd. The PXB mice were generated as described previously (Tateno et al., 2004). All PXB mice used in the present study were derived from the same donor cryopreserved hepatocytes (BD85, from a 5-year-old black male; BD Biosciences, Franklin Lakes, NJ). The blood concentration of human albumin in the PXB mice was measured according to a previous report (Tateno et al., 2004) to predict the replacement index of human hepatocytes that had repopulated in the host mouse liver. The actual values of the replacement index in PXB mice used in this study ranged from 82 to 94%.

Pharmacokinetic DDI Study in PXB Mice. Male PXB mice (11–12-weeks-old, 18–23 g) were used in this study. The suspensions of RIF prepared with corn oil were given intraperitoneally at doses of 2, 10, and 50 mg/kg to the PXB mice once daily for 4 days. After the 4 days of treatment of RIF, the PXB mice received a mixture of CYP3A4, CYP2C8, CYP2C9, and CYP2C19 substrate drugs orally via cassette dosing. The dosing mixture was prepared by adding a dimethyl sulfoxide solution of each drug to a 0.5% methylcellulose aqueous solution. The dose of each substrate drug was as follows: TRZ (CYP3A4 substrate), 5 mg/kg; ROS (CYP2C8 substrate), 1 mg/kg; WAR (CYP2C9 substrate), 0.1 mg/kg; and MEP (CYP2C19 substrate), 5 mg/kg. Blood samples were collected at 2 h after administration on days 1 and 4 and 0.5, 1, 2, 4, and 7 h on day 5. The blood samples were centrifuged, and the plasma samples obtained were stored at −80°C until the analysis. After blood sampling on day 5, the mice were euthanized, and a piece of the liver was collected and preserved in RNAlater solution (Invitrogen, Carlsbad, CA) to stabilize the RNA. The remaining liver tissue was frozen in liquid nitrogen and stored at −80°C until microsomal preparation.

RNA Isolation and Quantitative Reverse Transcription-PCR. Total RNA was extracted from the liver using an RNeasy Plus mini kit (QIAGEN, Hilden, Germany) and was reverse-transcribed to obtain cDNA using a PrimeScript RT reagent kit (Takara Bio, Shiga, Japan) according to the manufacturer's instructions. SYBR-PCR was performed using an ABI PRISM 7900HT (Invitrogen) with SYBR Premix Ex Taq (Takara Bio). The PCR conditions were as follows: after initial denaturation at 94°C for 5 min, the amplification was performed by denaturation at 94°C for 30 s, annealing at 65°C for 30 s, and extension at 72°C for 30 s for 45 cycles. In all cases, the input cDNA concentrations were normalized to those of glyceraldehyde-3-phosphate dehydrogenase (GAPDH; ΔCt). The relative mRNA expression was determined by a $2^{-\Delta\Delta Ct}$ calculation. The primer sequences used in the present study are summarized in Table 1. We confirmed that these primers were capable of amplifying human but not mouse genes.

Preparation of Liver Microsomes and Metabolic Assay. Liver microsomes were prepared from the frozen liver tissues as described previously (Sugihara et al., 2001). The reaction conditions for the enzyme activity of each P450 isoform are summarized in Table 2. The optimized substrate concentrations, the microsomal concentrations, and the reaction times were used to determine metabolic activity precisely. A reaction mixture (50 μl) consisted of 100 mM phosphate buffer, pH 7.4, 3 mM magnesium chloride, 8 mM G-6-P, 1 U/ml G-6-P-DH, 0.8 mM $NADP^+$, microsomal protein, and substrate. The reaction was initiated by the addition of an NADPH-generating system (a mixture of magnesium chloride, G-6-P, G-6-P-DH, and $NADP^+$) after preincubation of the mixture without the NADPH-generating system for 5 min at 37°C. The reaction was terminated at the designated time by the addition of ice-cold methanol containing propranolol as an internal standard. The sample was centrifuged, and the supernatant was diluted with water. The metabolite of each substrate was analyzed using a liquid chromatography-tandem mass spectrometry (LC/MS/MS) system.

Pretreatment of Plasma. Two microliters of plasma sample, 2 μl of dimethyl sulfoxide, and 30 μl of the ice-cold methanol containing the internal standard were mixed and centrifuged. The calibration standards were prepared in the same manner as the plasma samples. The supernatant was mixed with 10

TABLE 1

The sequences of the primers for SYBR-PCR

Gene Name	Primer Sequence (5′–3′)	
	Forward	Reverse
CYP1A2	AGCTTGACCTTCAGCACAGAC	GATAGTGCTCCTGGACTGTTTTC
CYP2B6	CACTCATCAGCTCTGTATTCGG	GTATGGCATTTTGGCTCGG
CYP2C8	CACAGCTAAAGTCCAGGAAGAG	GATGGGCTAGCATTCTTCAGAC
CYP2C9	ACTATCTCATTCCCAAGGGCAC	GTTCACTAGATCTTCAGGGAAGGG
CYP2C19	CAGCTGACTTACTTGGAGCTGG	CCTGCTGAGAAAGGCATGAAG
CYP2D6[a]	GGTGTGACCCATATGACATC	CTCCCCGAGGCATGCACG
CYP3A4	AGTTAATCCACTGTGACTTTGCCC	TGAGGATGGAATGCAAGAGG
UGT1A1	TGTTCCCACTTACTGCACAAC	CTTCAAATTCCTGGGATAGTGG
MDR1	GTATTCAACTATCCCACCCGAC	GAGCTGAGTTCCTTTGTCTCCTAC
MRP2	ACATGAGAGTTGGAGTCTACGG	GGATAACTGGCAAACCTGATAC
GAPDH	CCGAGCCACATCGCTCAGAC	ATGACGAACATGGGGGCATCAG

[a] From Katoh et al. (2005a).

mM ammonium acetate, and the mixture was injected into the LC/MS/MS system.

LC/MS/MS Analysis. The concentrations of the substrate drugs (in plasma samples), and metabolites (in microsomal samples) were measured using the LC/MS/MS system consisting of an ACQUITY UPLC (Waters, Inc., Bedford, MA) connected to a 4000 QTRAP mass spectrometer (AB Sciex, Foster City, CA).

For the plasma samples, chromatographic separation was performed on a CAPCELL PAK C18 MGII column (3 μm, 3 mm inner diameter $\times$ 35 mm; Shiseido, Tokyo, Japan) using an injection volume of 10 μl (ROS and WAR) or 25 μl (TRZ and MEP) and a run time of 4 min. The elution was conducted at a flow rate of 0.8 ml/min by a linear gradient with the mobile phase, which consisted of 10 mM ammonium acetate in water (A) and methanol (B). The gradient condition of B (%) was as follows: at 0, 0.2, 2.2, 2.21, 3, and 3.01 min, the B% was 80, 80, 25, 10, 10, and 80%, respectively. The mass spectrometry detection was performed by positive ionization electrospray. The multiple reaction monitoring mode was used, and the monitor ions (*m/z* precursor ion > product ion) were as follows: ROS (358.1 > 153.3), WAR (309.6 > 163.5), TRZ (343.4 > 308.1), and MEP (219.6 > 134.4). The plasma concentration ranges of quantification were as follows: ROS (1.07–3570 ng/ml), WAR (0.925–9250 ng/ml), TRZ (0.343–3430 ng/ml), and MEP (2.18–6550 ng/ml).

For the microsomal samples, chromatographic separation was performed on an ACQUITY UPLC BEH C18 column (1.7 μm, 2.1 mm inner diameter $\times$ 50 mm; Waters, Milford, MA) using an injection volume of 7.5 μl and a run time of 2.5 min. The elution was conducted at a flow rate of 0.5 ml/min by a linear gradient with the mobile phase, which consisted of 10 mM ammonium acetate in water (A for CYP1A2, CYP2B6, CYP2C9 (7-hydroxywarfarin), CYP2C19, and CYP2D6 assays) or 0.05% formic acid in water (A for CYP2C8, CYP2C9 (4′-hydroxydiclofenac), and CYP3A4 assays) and methanol (B). The gradient condition of B (%) was as follows: at 0, 0.2, 1.5, 2 and 2.01 min, the B% was 95, 95, 5, 5, and 95%, respectively. The mass spectrometry detection was performed by positive ionization electrospray. The multiple reaction monitoring mode was used, and the monitor ions (*m/z* precursor ion > product ion) were as follows: CYP1A2 (acetaminophen, 152.0 > 110.0), CYP2B6 (hydroxybupropion, 256.1 > 238.1), CYP2C8 (*N*-demethyl rosiglitazone, 344.1 > 121.1; 5-hydroxyrosiglitazone, 374.1 > 151.1), CYP2C9 (4′-hydroxydiclofenac, 312.05 > 230.45; 7-hydroxywarfarin, 325.6 > 163.5), CYP2C19 (4′-hydroxymephenytoin, 235.0 > 150.15), CYP2D6 (dextrorphan, 258.1 > 157.1), and CYP3A4 (1′-hydroxytriazolam, 359.1 > 176.1; 4-hydroxytriazolam, 359.1 > 314.1). Although the metabolites concentrations in the microsomal samples were not quantified, we have confirmed the linearity of signal intensities and no signals in the blank samples.

Pharmacokinetic Analysis. The pharmacokinetic parameters for TRZ, ROS, WAR, and MEP were obtained by a noncompartmental analysis. The log-transformed plasma concentrations were plotted against time. The slope of the elimination phase (λ_z) was estimated by linear regression. The maximal plasma concentration (C_{max}) and time to C_{max} (t_{max}) were obtained directly from the observed values. The apparent $t_{1/2}$ was obtained as $\ln 2/\lambda_z$. The area under the plasma concentration-time curve (AUC) from time 0 to the last data point (AUC_{0-t}) was calculated using the linear trapezoidal method. The AUC after the last data point ($AUC_{\lambda z}$) was estimated by extrapolating with λ_z. The sum of AUC_{0-t} and $AUC_{\lambda z}$ was regarded as $AUC_{0-\infty}$.

Statistical Analysis. A one-way analysis of variance with a Dunnett's test was performed to assess for significant differences in the pharmacokinetics, metabolic activity in the liver microsomes, and mRNA expression in the liver between vehicle- and RIF-treated groups. The statistical analyses were performed using the SAS software program (SAS Institute, Cary, NC). The criterion for statistical significance was $P < 0.05$.

Results

The Effect of RIF Treatment on the Pharmacokinetics of CYP3A4 and CYP2C Substrate Drugs. The pharmacokinetics of CYP3A4 (TRZ) and CYP2C substrate drugs (ROS, MEP, and WAR) was evaluated after repeated intraperitoneal administration of RIF (2, 10, and 50 mg/kg daily for 4 days) or vehicle to the PXB mice. The plasma concentration-time profiles of the substrate drugs are shown in Fig. 1, and the pharmacokinetic parameters and the AUC decrease (percentage) of substrate drugs are summarized in Table 3. The plasma exposure to TRZ was decreased with increased doses of RIF

TABLE 2

The reaction conditions for P450 enzyme assay using the liver microsomes

P450	Substrate	Metabolite	Substrate Concentration	Microsomal Concentration	Reaction Time
			μM	*mg/ml*	*min*
CYP1A2	Phenacetin	Acetaminophen	5	0.5	20
CYP2B6	Bupropion	Hydroxybupropion	5	0.5	20
CYP2C8	Rosiglitazone	*N*-Demethylrosiglitazone 5-Hydroxyrosiglitazone	2	0.2	20
CYP2C9	(*S*)-Warfarin	7-Hydroxywarfarin	4	1	30
	Diclofenac	4′-Hydroxydiclofenac	4	0.2	30
CYP2C19	(*S*)-(−)-Mephenytoin	4′-Hydroxymephenytoin	20	0.5	20
CYP2D6	Dextromethorphan	Dextrorphan	1	0.2	20
CYP3A4	Triazolam	1′-Hydroxytriazolam 4-Hydroxytriazolam	2	0.2	20

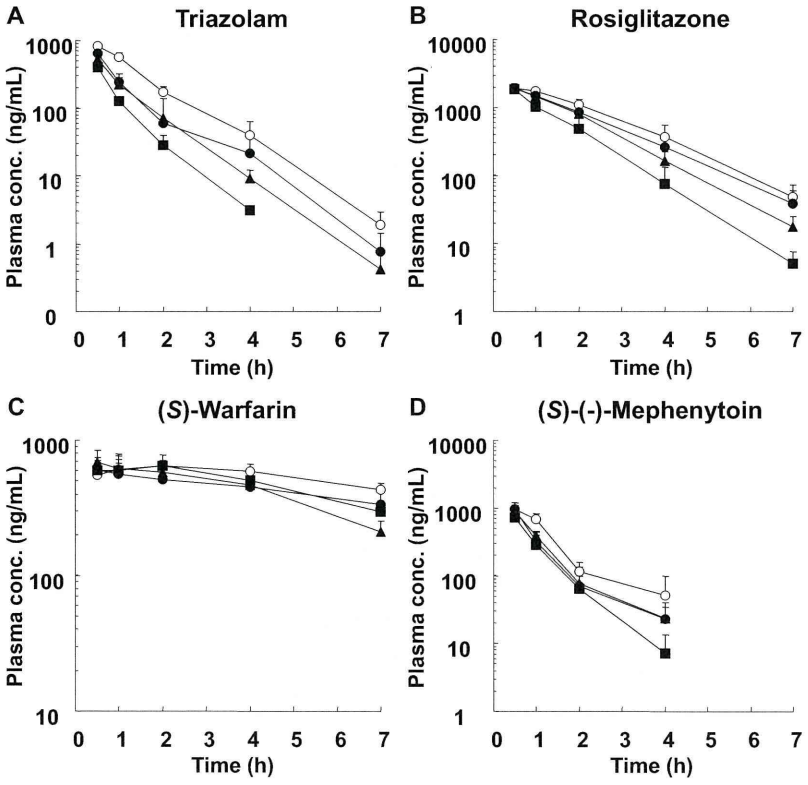

FIG. 1. The plasma concentration-time profiles of TRZ (A), ROS (B), WAR (C), and MEP (D) after repeated intraperitoneal administration of RIF once daily for 4 days to male PXB mice. The PXB mice were given oral doses of 5 mg/kg TRZ (CYP3A4 substrate), 1 mg/kg ROS (CYP2C8 substrate), 0.1 mg/kg WAR (CYP2C9 substrate), and 5 mg/kg MEP (CYP2C19 substrate) via cassette dosing after 4 days of treatment with 2 (●), 10 (▲), or 50 (■) mg/kg RIF or vehicle (○). Each point represents the mean ± S.D. of three mice.

(Fig. 1A). The TRZ AUC was significantly decreased by 46 (2 mg/kg), 54 (10 mg/kg), and 71% (50 mg/kg) compared with the vehicle control (Table 3). RIF treatment also resulted in an AUC decrease of ROS and MEP with increased doses of RIF, and the statistically significance in the AUC decrease was observed only at the dose of 50 mg/kg RIF as 47% for ROS and 46% for MEP (Fig. 1, B and D; Table 3). Treatment with RIF had no effect on the pharmacokinetics of WAR (Fig. 1C; Table 3).

The Metabolic Activities of Human P450 Enzymes in the Liver Microsomes. The metabolic activities of seven human P450 enzymes were determined in the liver microsomes prepared from PXB mice treated with RIF. The fold-induction of enzyme activity for each P450 isoform in the RIF-treated group is shown in Fig. 2. The metabolic activities of CYP3A4 (1′- and 4-hydroxy-TRZ), CYP2C8 (5-hydroxy- and *N*-demethyl-ROS), and CYP2C19 (4-hydroxy-MEP), whose induction was detected in the in vivo study, were significantly increased with increased doses of RIF. Although CYP2C9 induction was not detected in the in vivo study, the metabolic activity of CYP2C9 (7-hydroxy-WAR and 4′-hydroxydiclofenac) was significantly increased by RIF treatment. In addition to CYP3A4 and CYP2C enzymes, the metabolic activities of the CYP1A2, CYP2B6, and CYP2D6 enzymes were also examined. The metabolic activity of CYP2B6 (hydroxybupropion) but not CYP1A2 (acetaminophen) or CYP2D6 (dextrorphan) was increased in a dose-dependent manner by RIF.

TABLE 3

The pharmacokinetic parameters of TRZ, ROS, WAR, and MEP administered orally in cassette dosing after repeated intraperitoneal administration of RIF once daily for 4 days to the male PXB mice

Each value was determined from the data shown in Fig. 1. Data represent the mean ± S.D. of three mice.

		RIF Dose	C_{max}	$t_{1/2}$	$AUC_{0-\infty}$	AUC Decrease
		mg/kg	*ng/ml*	*h*	*ng · h/ml*	*%*
CYP3A4	TRZ	Vehicle	824 ± 92	0.733 ± 0.066	1210 ± 110	
		2	643 ± 72*	0.775 ± 0.055	650 ± 117**	46
		10	408 ± 45**	0.699 ± 0.109	561 ± 205***	54
		50	531 ± 43***	0.575 ± 0.028	346 ± 27***	71
CYP2C8	ROS	Vehicle	1970 ± 240	1.07 ± 0.13	4960 ± 770	
		2	1920 ± 210	1.10 ± 0.18	4120 ± 680	17
		10	1900 ± 350	0.911 ± 0.075	3690 ± 860	26
		50	1850 ± 330	0.772 ± 0.058	2630 ± 900*	47
CYP2C9	WAR	Vehicle	680 ± 26	ND	3830 ± 60	
		2	640 ± 161	ND	3120 ± 830	19
		10	709 ± 197	ND	3420 ± 610	11
		50	715 ± 5	ND	3160 ± 400	18
CYP2C19	MEP	Vehicle	951 ± 250	0.757 ± 0.249	1240 ± 230	
		2	955 ± 150	0.683 ± 0.144	844 ± 173	32
		10	894 ± 102	0.660 ± 0.155	876 ± 84	30
		50	730 ± 61	0.524 ± 0.120	685 ± 198*	46

ND, not determined.
Statistically significant from the vehicle-treated group: * $P < 0.05$; ** $P < 0.01$; *** $P < 0.001$.

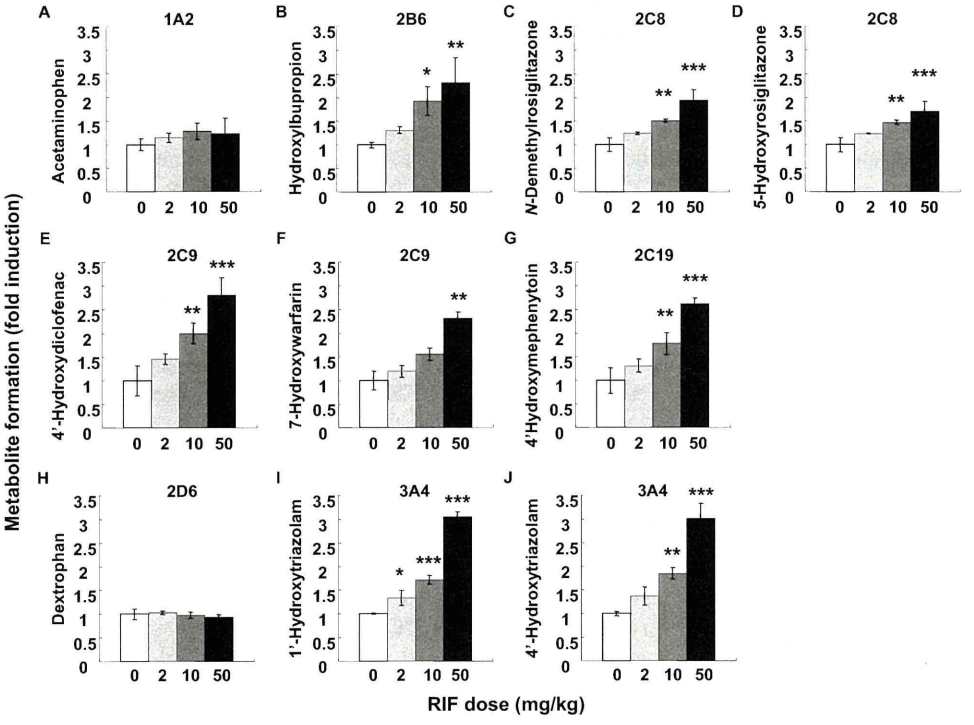

FIG. 2. The metabolic activities of P450 enzymes in the liver microsomes prepared from PXB mice. The liver microsomes were prepared from RIF- or vehicle-treated PXB mice. The activities of P450 enzymes, CYP1A2 (A), CYP2B6 (B), CYP2C8 (C and D), CYP2C9 (E and F), CYP2C19 (G), CYP2D6 (H), and CYP3A4 (I and J), were determined. The experimental conditions are summarized in Table 2. The fold induction in the RIF-treated group compared with vehicle-treated group was calculated. The metabolic activity of each of the mouse liver microsomes was determined from the means of duplicate assay. Each bar represents the mean ± S.D. of three mice. Statistically significant from the vehicle-treated group; *, $P < 0.05$, **, $P < 0.01$, and ***, $P < 0.001$.

The mRNA Expression of Human P450 Enzymes and Transporters. The mRNA expression of the seven human P450 enzymes, UGT1A1, and transporters, including MDR1 and MRP2, was evaluated in the livers of the PXB mice treated with RIF. The fold induction of mRNA expression of enzymes and transporters in the RIF-treated group is shown in Fig. 3. The magnitude of CYP3A4 induction was the largest among the P450 enzymes, followed by CYP2C8 and CYP2B6. Although the enzyme activities of CYP2C9 and CYP2C19 were increased by RIF treatment, the increase in mRNA expression was too slight to detect significant difference. No changes in the mRNA expression of CYP1A2 and CYP2D6 were observed. RIF treatment significantly increased the mRNA expression of UGT1A1, but not MDR1 and MRP2.

Discussion

In the present study, in vivo study using PXB mice, we simultaneously investigated the inductive effect of RIF on CYP3A4 and CYP2C enzymes. We demonstrated that concomitant use of RIF

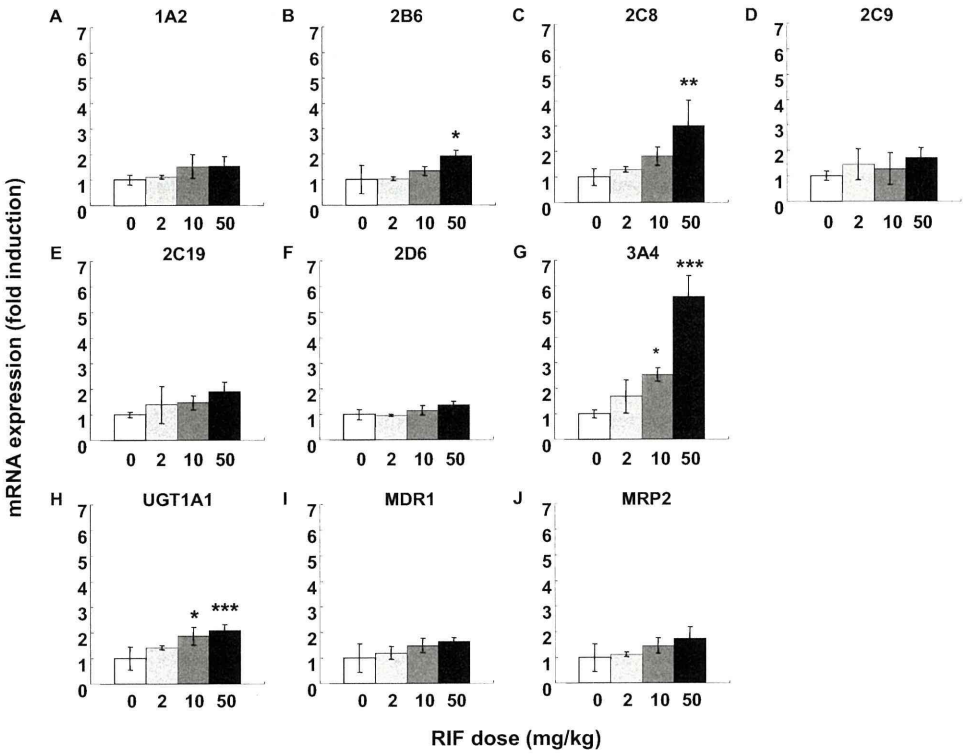

FIG. 3. The mRNA expression levels of P450 enzymes and drug transporters in the liver of PXB mice. The mRNA expression levels of CYP1A2 (A), CYP2B6 (B), CYP2C8 (C), CYP2C9 (D), CYP2C19 (E), CYP2D6 (F), CYP3A4 (G), UGT1A1 (H), MDR1 (I), and MRP2 (J) were determined by SYBR-PCR. The mRNA expression level of each gene was normalized to that of GAPDH. The fold induction in the RIF-treated group compared with vehicle-treated group was calculated. Each bar represents the mean ± S.D. of three mice. Statistically significant from the vehicle-treated group; *, $P < 0.05$, **, $P < 0.01$, and ***, $P < 0.001$.

affects the pharmacokinetics of both CYP3A4 and CYP2C substrate drugs and that the inductive effect of RIF on CYP3A4 is greater than that on CYP2C enzymes. In addition, in vitro studies using the liver samples after RIF treatment were also carried out to examine the enzyme activities of human P450s and the mRNA expression levels of human P450s, UGT, and transporters. The induction by RIF was observed in the genes whose expression levels were known to be regulated by the human PXR, but no change was observed in the genes not regulated by the PXR (CYP2D6).

To compare the pharmacokinetic data between studies conducted in humans and this study, we selected substrate drugs that have previously been reported to have DDIs with RIF in humans. In a clinical study, the AUC decreases in the P450 substrate drug with concomitant use of RIF (600 mg daily) were 46 to 78% (ROS), 57 to 85% (WAR), and 95% (TRZ) (Villikka et al., 1997; Niemi et al., 2003, 2004; Park et al., 2004). The DDI information on CYP2C19 substrate drugs is very limited, and we could only find information about the urinary excretion data for 4′-hydroxymephenytoin, the main metabolite of MEP (Zhou et al., 1990; Feng et al., 1998). The concomitant use of RIF (600 mg daily) increased the urinary excretion of 4′-hydroxymephenytoin from 1.4- to 2.8-fold (Zhou et al., 1990). Assuming that the urinary excretion amount of the metabolite reflects the metabolic clearance of MEP, the decrease in the AUC would be between 29 to 64% as a result of RIF treatment. These reported clinical data suggest that CYP3A4 is the most susceptible to induction by RIF treatment and that the magnitude of induction of CYP2C8, CYP2C9, and CYP2C19 by RIF seems to be relatively weak compared with CYP3A4. In this study using PXB mice, RIF treatment resulted in the largest AUC decrease in TRZ, followed by ROS and MEP (Fig. 1; Table 3). The response to RIF treatment observed in the PXB mice is therefore similar to that in humans.

It was unexpected that the exposure to WAR was not affected by RIF treatment, despite CYP2C9 induction in the liver microsomes (Figs. 1C and 2, E and F; Table 3). The elimination pathways of WAR other than metabolism by CYP2C9 might have made it harder to detect CYP2C9 induction in the in vivo study. In humans, WAR is mainly metabolized to the 7-hydroxyl metabolite by CYP2C9, although WAR is also metabolized to other hydroxyl metabolites by other P450 isoforms (Inoue et al., 2009). Given that the PXB mice used in the present study were derived from the hepatocytes of a single donor, the contribution of CYP2C9 to WAR metabolism in these PXB mice might not be uniformly typical of humans in general. The availability of murine P450 isoforms remaining in the liver of PXB mice could also potentially have affected the overall metabolism of WAR in the in vivo study.

We measured the metabolic activities of WAR in the liver microsomes of SCID (severe combined immunodeficiency) mice (the background strain of the PXB mice) and in pooled human liver microsomes to compare them with PXB mice (supplemental figure). The three types of hydroxyl metabolites of WAR, including 7-hydroxy-WAR, were detected in all of the microsomes. However, the 7-hydroxylation activity in the liver microsomes of PXB mice was only one fifth of that in the human liver microsomes. Therefore, the contribution of CYP2C9 to WAR metabolism in the PXB mice may have been smaller than expected. In fact, the formation of another hydroxyl WAR (M2) in the liver microsomes of SCID mice was greater than that in the human liver microsomes, although the absolute metabolic clearance was not determined (supplemental figure). The metabolic activity of murine P450s remaining in the liver could possibly make it difficult to examine CYP2C9 induction by examining the pharmacokinetics of WAR.

To investigate whether a genetic polymorphism could explain the lower CYP2C9 activity in PXB mice, the CYP2C9 genomic polymorphism was determined by Invader assay (BML, Inc., Tokyo, Tokyo) for the cryopreserved human hepatocytes (lot BD85) used in this study. Although no variant sequence was detected in the CYP2C9 gene (data not shown), real-time quantitative reverse transcription-PCR analysis revealed that the mRNA expression level of CYP2C9 in the hepatocytes was relatively low compared with that in other donor hepatocytes (data not shown). In fact, the plasma elimination of WAR in this study seems to be slower than that in the previous study using PXB mice transplanted with a different lot of human hepatocytes (Inoue et al., 2008). Therefore, the main reason for the failure to detect of CYP2C9 induction in the in vivo study was probably the low hepatic expression of CYP2C9 in the PXB mice used in this study.

In humans, a therapeutic dose of RIF (600 mg) resulted in an $AUC_{0-\infty}$ of 22,400 to 35,300 ng · h/ml (Polk et al., 2001), which was a similar range of plasma exposure as the PXB mouse receiving the 10 mg/kg RIF (M. Kakuni, unpublished data). Considering the AUC decrease of the substrate drugs in PXB mice and humans caused by RIF treatment, the inductive response in PXB mice seems to be relatively weaker than that in humans. It has been reported that CYP3A4, CYP2C8, CYP2C9, and CYP2C19 are expressed in the human intestine (Kolars et al., 1992; Läpple et al., 2003; van de Kerkhof et al., 2008). In addition, it is well known that drug metabolism by intestinal CYP3A4 affects the pharmacokinetics of orally administered drugs (Kato et al., 2003). RIF was previously reported to induce CYP3A4 not only in the liver but also in the intestine in humans (Kolars et al., 1992; van de Kerkhof et al., 2008). Therefore, the decrease in the AUC by concomitant use of RIF in the clinic is accounted for by induction of P450 enzymes both in the liver and in the intestine. In PXB mice, only the liver, but not the intestine, is humanized. Therefore, the intestinal P450 enzymes in PXB mice cannot be induced by RIF, which is a specific human PXR ligand. As a result of the lack of induction in the intestinal P450 enzymes in PXB mice, the reduction of the AUC in the PXB mice would be predicted to be smaller than that in humans. In addition, the hepatic exposure of PXB mice to RIF might be smaller than the expected level, because RIF was administered intraperitoneally, not orally, to PXB mice in this study. The relatively low exposure of the liver to RIF may have result in a weaker induction in the PXB mice.

The induction of CYP3A4 and CYP2C8, CYP2C9, and CYP2C19 by RIF in PXB mice was also demonstrated by examining the enzyme activities using typical substrates for each P450 isoform (Fig. 2). The induction of CYP2B6 in the liver microsomes was also detected (Fig. 2B). This result is consistent with the fact that the expression of CYP2B6 is regulated by the human PXR (Sinz et al., 2008). Next, we determined the mRNA expression levels of other genes, including UGT1A1, MDR1, and MRP2, whose expression levels are also under the regulation of the human PXR (Fig. 3) (Nakata et al., 2006). It was previously demonstrated that RIF led to a small increase in the mRNA expression of these genes using human hepatocytes (Nishimura et al., 2008a,b). In this study, the mRNA expression levels seemed to be slightly increased by RIF in a dose-dependent manner. Statistically significant increase was observed in the mRNA expression levels of UGT1A1 but not in those of MDR1 or MRP2 expression (Fig. 3, H–J). These results might be also attributed to the use of single donor hepatocytes as discussed above.

In the present study, we have performed a DDI study focusing on the human PXR-related induction of CYP3A4 and CYP2C enzymes simultaneously by using the cassette dosing of substrate drugs in PXB mice. We have demonstrated that the PXB mice show a similar response to humans in terms of human PXR-related P450 induction by

RIF. Because the PXB mice used in the present study were derived from the hepatocytes of a single donor, further studies are needed to generalize the present findings by performing DDI studies using PXB mice derived from the different hepatocyte donors.

Considering the magnitude of induction and its contribution to the drug metabolism in clinical situations, CYP3A4 is the most important enzyme to examine during the preclinical development of a new drug candidate. Several groups have established PXR and/or CYP3A4 humanized mice using gene knockout and transgenic techniques (Xie et al., 2000; Ma et al., 2007; Kim et al., 2008; Scheer et al., 2008; Hasegawa et al., 2011). On the other hand, the previous and present DDI studies have demonstrated that the induction of CYP2C enzymes also has a large impact on the pharmacokinetics of CYP2C substrate drugs (Niemi et al., 2003). At present, chimeric mice with a humanized liver, including the PXB mice, are only animal model available to investigate DDIs caused by the induction of CYP2C together with CYP3A4. Furthermore, several groups have reported that the drug-metabolizing profiles in PXB mice are similar to those in humans (Kamimura et al., 2010). Therefore, PXB mice seem to be a suitable animal model to examine the enzyme induction by a drug and its metabolite(s) if these are ligands for the human PXR. In conclusion, PXB mice will provide the opportunity to examine potential DDIs caused by PXR-related enzyme induction in a situation similar to that observed in humans.

Acknowledgments

We thank Tatsuya Matsumi and Dr. Saburo Sugai for supporting this research and reviewing the manuscript.

Authorship Contributions

Participated in research design: Hasegawa and Tahara.

Conducted experiments: Hasegawa, Tahara, Inoue, Kakuni, and Tateno.

Performed data analysis: Hasegawa.

Wrote or contributed to the writing of the manuscript: Hasegawa, Tahara, and Ushiki.

References

Chen Y and Goldstein JA (2009) The transcriptional regulation of the human CYP2C genes. *Curr Drug Metab* **10:**567–578.

Cui X, Thomas A, Gerlach V, White RE, Morrison RA, and Cheng KC (2008) Application and interpretation of hPXR screening data: validation of reporter signal requirements for prediction of clinically relevant CYP3A4 inducers. *Biochem Pharmacol* **76:**680–689.

de Wildt SN, Kearns GL, Leeder JS, and van den Anker JN (1999) Cytochrome P450 3A: ontogeny and drug disposition. *Clin Pharmacokinet* **37:**485–505.

Dixit V, Hariparsad N, Li F, Desai P, Thummel KE, and Unadkat JD (2007) Cytochrome P450 enzymes and transporters induced by anti-human immunodeficiency virus protease inhibitors in human hepatocytes: implications for predicting clinical drug interactions. *Drug Metab Dispos* **35:**1853–1859.

Feng HJ, Huang SL, Wang W, and Zhou HH (1998) The induction effect of rifampicin on activity of mephenytoin 4′-hydroxylase related to M1 mutation of CYP2C19 and gene dose. *Br J Clin Pharmacol* **45:**27–29.

Hasegawa M, Kapelyukh Y, Tahara H, Seibler J, Rode A, Krueger S, Lee DN, Wolf CR, and Scheer N (2011) Quantitative prediction of human pregnane X receptor and cytochrome P450 3A4 mediated drug-drug interaction in a novel multiple humanized mouse line. *Mol Pharmacol* **80:**518–528.

Inoue T, Nitta K, Sugihara K, Horie T, Kitamura S, and Ohta S (2008) CYP2C9-catalyzed metabolism of *S*-warfarin to 7-hydroxywarfarin in vivo and in vitro in chimeric mice with humanized liver. *Drug Metab Dispos* **36:**2429–2433.

Inoue T, Sugihara K, Ohshita H, Horie T, Kitamura S, and Ohta S (2009) Prediction of human disposition toward *S*-3*H*-warfarin using chimeric mice with humanized liver. *Drug Metab Pharmacokinet* **24:**153–160.

Jones SA, Moore LB, Shenk JL, Wisely GB, Hamilton GA, McKee DD, Tomkinson NC, LeCluyse EL, Lambert MH, Willson TM, et al. (2000) The pregnane X receptor: a promiscuous xenobiotic receptor that has diverged during evolution. *Mol Endocrinol* **14:**27–39.

Kamiguchi N, Aoyama E, Okuda T, and Moriwaki T (2010) A 96-well plate assay for CYP4503A induction using cryopreserved human hepatocytes. *Drug Metab Dispos* **38:**1912–1916.

Kamimura H, Nakada N, Suzuki K, Mera A, Souda K, Murakami Y, Tanaka K, Iwatsubo T, Kawamura A, and Usui T (2010) Assessment of chimeric mice with humanized liver as a tool for predicting circulating human metabolites. *Drug Metab Pharmacokinet* **25:**223–235.

Kanebratt KP and Andersson TB (2008) HepaRG cells as an in vitro model for evaluation of cytochrome P450 induction in humans. *Drug Metab Dispos* **36:**137–145.

Kato M, Chiba K, Hisaka A, Ishigami M, Kayama M, Mizuno N, Nagata Y, Takakuwa S, Tsukamoto Y, Ueda K, et al. (2003) The intestinal first-pass metabolism of substrates of CYP3A4 and P-glycoprotein-quantitative analysis based on information from the literature. *Drug Metab Pharmacokinet* **18:**365–372.

Katoh M, Matsui T, Nakajima M, Tateno C, Soeno Y, Horie T, Iwasaki K, Yoshizato K, and Yokoi T (2005a) In vivo induction of human cytochrome P450 enzymes expressed in chimeric mice with humanized liver. *Drug Metab Dispos* **33:**754–763.

Katoh M, Watanabe M, Tabata T, Sato Y, Nakajima M, Nishimura M, Naito S, Tateno C, Iwasaki K, Yoshizato K, et al. (2005b) In vivo induction of human cytochrome P450 3A4 by rifabutin in chimeric mice with humanized liver. *Xenobiotica* **35:**863–875.

Kim S, Dinchuk JE, Anthony MN, Orcutt T, Zoeckler ME, Sauer MB, Mosure KW, Vuppugalla R, Grace JE Jr, Simmermacher J, et al. (2010) Evaluation of cynomolgus monkey pregnane X receptor, primary hepatocyte, and in vivo pharmacokinetic changes in predicting human CYP3A4 induction. *Drug Metab Dispos* **38:**16–24.

Kim S, Pray D, Zheng M, Morgan DG, Pizzano JG, Zoeckler ME, Chimalakonda A, and Sinz MW (2008) Quantitative relationship between rifampicin exposure and induction of Cyp3a11 in SXR humanized mice: extrapolation to human CYP3A4 induction potential. *Drug Metab Lett* **2:**169–175.

Kolars JC, Schmiedlin-Ren P, Schuetz JD, Fang C, and Watkins PB (1992) Identification of rifampin-inducible P450IIIA4 (CYP3A4) in human small bowel enterocytes. *J Clin Invest* **90:**1871–1878.

Läpple F, von Richter O, Fromm MF, Richter T, Thon KP, Wisser H, Griese EU, Eichelbaum M, and Kivistö KT (2003) Differential expression and function of CYP2C isoforms in human intestine and liver. *Pharmacogenetics* **13:**565–575.

LeCluyse EL (2001) Pregnane X receptor: molecular basis for species differences in CYP3A induction by xenobiotics. *Chem Biol Interact* **134:**283–289.

Luo G, Guenthner T, Gan LS, and Humphreys WG (2004) CYP3A4 induction by xenobiotics: biochemistry, experimental methods and impact on drug discovery and development. *Curr Drug Metab* **5:**483–505.

Ma X, Shah Y, Cheung C, Guo GL, Feigenbaum L, Krausz KW, Idle JR, and Gonzalez FJ (2007) The PREgnane X receptor gene-humanized mouse: a model for investigating drug-drug interactions mediated by cytochromes P450 3A. *Drug Metab Dispos* **35:**194–200.

Nakata K, Tanaka Y, Nakano T, Adachi T, Tanaka H, Kaminuma T, and Ishikawa T (2006) Nuclear receptor-mediated transcriptional regulation in Phase I, II, and III xenobiotic metabolizing systems. *Drug Metab Pharmacokinet* **21:**437–457.

Niemi M, Backman JT, Fromm MF, Neuvonen PJ, and Kivistö KT (2003) Pharmacokinetic interactions with rifampicin: clinical relevance. *Clin Pharmacokinet* **42:**819–850.

Niemi M, Backman JT, and Neuvonen PJ (2004) Effects of trimethoprim and rifampin on the pharmacokinetics of the cytochrome P450 2C8 substrate rosiglitazone. *Clin Pharmacol Ther* **76:**239–249.

Nishimura M, Koeda A, Morikawa H, Satoh T, Narimatsu S, and Naito S (2008a) Comparison of inducibility of multidrug resistance (MDR)1, multidrug resistance-associated protein (MRP)1, and MRP2 mRNAs by prototypical microsomal enzyme inducers in primary cultures of human and cynomolgus monkey hepatocytes. *Biol Pharm Bull* **31:**2068–2072.

Nishimura M, Koeda A, Shimizu T, Nakayama M, Satoh T, Narimatsu S, and Naito S (2008b) Comparison of inducibility of sulfotransferase and UDP-glucuronosyltransferase mRNAs by prototypical microsomal enzyme inducers in primary cultures of human and cynomolgus monkey hepatocytes. *Drug Metab Pharmacokinet* **23:**45–53.

Park JY, Kim KA, Kang MH, Kim SL, and Shin JG (2004) Effect of rifampin on the pharmacokinetics of rosiglitazone in healthy subjects. *Clin Pharmacol Ther* **75:**157–162.

Polk RE, Brophy DF, Israel DS, Patron R, Sadler BM, Chittick GE, Symonds WT, Lou Y, Kristoff D, and Stein DS (2001) Pharmacokinetic Interaction between amprenavir and rifabutin or rifampin in healthy males. *Antimicrob Agents Chemother* **45:**502–508.

Raucy JL, Mueller L, Duan K, Allen SW, Strom S, and Lasker JM (2002) Expression and induction of CYP2C P450 enzymes in primary cultures of human hepatocytes. *J Pharmacol Exp Ther* **302:**475–482.

Scheer N, Ross J, Rode A, Zevnik B, Niehaves S, Faust N, and Wolf CR (2008) A novel panel of mouse models to evaluate the role of human pregnane X receptor and constitutive androstane receptor in drug response. *J Clin Invest* **118:**3228–3239.

Shin HC, Kim HR, Cho HJ, Yi H, Cho SM, Lee DG, Abd El-Aty AM, Kim JS, Sun D, and Amidon GL (2009) Comparative gene expression of intestinal metabolizing enzymes. *Biopharm Drug Dispos* **30:**411–421.

Sinz M, Wallace G, and Sahi J (2008) Current industrial practices in assessing CYP450 enzyme induction: preclinical and clinical. *AAPS J* **10:**391–400.

Strom SC, Davila J, and Grompe M (2010) Chimeric mice with humanized liver: tools for the study of drug metabolism, excretion, and toxicity. *Methods Mol Biol* **640:**491–509.

Sugihara K, Kitamura S, Yamada T, Ohta S, Yamashita K, Yasuda M, and Fujii-Kuriyama Y (2001) Aryl hydrocarbon receptor (AhR)-mediated induction of xanthine oxidase/xanthine dehydrogenase activity by 2,3,7,8-tetrachlorodibenzo-p-dioxin. *Biochem Biophys Res Commun* **281:**1093–1099.

Tateno C, Yoshizane Y, Saito N, Kataoka M, Utoh R, Yamasaki C, Tachibana A, Soeno Y, Asahina K, Hino H, et al. (2004) Near completely humanized liver in mice shows human-type metabolic responses to drugs. *Am J Pathol* **165:**901–912.

van de Kerkhof EG, de Graaf IA, Ungell AL, and Groothuis GM (2008) Induction of metabolism and transport in human intestine: validation of precision-cut slices as a tool to study induction of drug metabolism in human intestine in vitro. *Drug Metab Dispos* **36:**604–613.

Villikka K, Kivistö KT, Backman JT, Olkkola KT, and Neuvonen PJ (1997) Triazolam is ineffective in patients taking rifampin. *Clin Pharmacol Ther* **61:**8–14.

Xie W, Barwick JL, Downes M, Blumberg B, Simon CM, Nelson MC, Neuschwander-Tetri BA, Brunt EM, Guzelian PS, and Evans RM (2000) Humanized xenobiotic response in mice expressing nuclear receptor SXR. *Nature* **406:**435–439.

Zhou HH, Anthony LB, Wood AJ, and Wilkinson GR (1990) Induction of polymorphic 4′-hydroxylation of *S*-mephenytoin by rifampicin. *Br J Clin Pharmacol* **30:**471–475.

Address correspondence to: Dr. Maki Hasegawa, Kyowa Hakko Kirin Co., Ltd., 1188 Shimotogari, Nagaizumi-cho, Sunto-gun, Shizuoka, 411-8731, Japan. E-mail: maki.hasegawa@kyowa-kirin.co.jp

Cytokine 56 (2011) 564–572

Contents lists available at SciVerse ScienceDirect

Cytokine

journal homepage: www.elsevier.com/locate/issn/10434666

Interferon regulatory factor-4 activates IL-2 and IL-4 promoters in cooperation with c-Rel

Hisakazu Shindo [a,c,1], Kiyoshi Yasui [a,1], Kazuo Yamamoto [a,e], Kiri Honma [b], Katsuyuki Yui [b], Tomoko Kohno [a], Yuhua Ma [a], Koon Jiew Chua [a], Yoshinao Kubo [a], Hitoshi Aihara [d], Takashi Ito [d], Takeshi Nagayasu [c], Toshifumi Matsuyama [a,*], Hideki Hayashi [a]

[a] Division of Cytokine Signaling, Department of Molecular Microbiology and Immunology, Nagasaki University Graduate School of Biomedical Sciences, 1-12-4 Sakamoto, Nagasaki 852-8523, Japan
[b] Division of Immunology, Department of Molecular Microbiology and Immunology, Nagasaki University Graduate School of Biomedical Sciences, 1-12-4 Sakamoto, Nagasaki 852-8523, Japan
[c] Division of Surgical Oncology, Department of Translational Medical Sciences, Nagasaki University Graduate School of Biomedical Sciences, 1-12-4 Sakamoto, Nagasaki 852-8523, Japan
[d] Department of Biochemistry, Nagasaki University Graduate School of Biomedical Sciences, 1-12-4 Sakamoto, Nagasaki 852-8523, Japan
[e] The Campbell Family Cancer Research Institute, 620 University Avenue, Suite 706, Toronto, Ontario M5G 2C1, Canada

ARTICLE INFO

Article history:
Received 6 January 2011
Received in revised form 15 July 2011
Accepted 3 August 2011
Available online 3 September 2011

Keywords:
Interferon regulatory factor (IRF)-4
c-Rel
IL-4
IL-2
Adult T-cell leukemia/lymphoma (ATLL)

ABSTRACT

Interferon regulatory factor (IRF)-4 is a member of the IRF transcription factor family, whose expression is primarily restricted to lymphoid and myeloid cells. In T-cells, IRF-4 expression is induced by T-cell receptor (TCR) cross-linking or treatment with phorbol-12-myristate-13-acetate (PMA)/Ionomycin, and IRF-4 is thought to be a critical factor for various functions of T-cells. To elucidate the IRF-4 functions in human adult T-cell leukemia virus type 1 (HTLV-1)-infected T-cells, which constitutively express IRF-4, we isolated IRF-4-binding proteins from T-cells, using a tandem affinity purification (TAP)-mass spectrometry strategy. Fourteen proteins were identified in the IRF-4-binding complex, including endogenous IRF-4 and the nuclear factor-kappaB (NF-κB) family member, c-Rel. The specific association of IRF-4 with c-Rel was confirmed by immunoprecipitation experiments, and IRF-4 was shown to enhance the c-Rel-dependent binding and activation of the interleukin-4 (IL-4) promoter region. We also demonstrated that IL-2 production was also enhanced by exogenously-expressed IRF-4 and c-Rel in the presence of P/I, in T-cells, and that the optimal IL-2 and IL-4 productions *in vivo* was IRF-4-dependent using IRF-$4^{-/-}$ mice. These data provide molecular evidence to support the clinical observation that elevated expression of c-Rel and IRF-4 is associated with the prognosis in adult T-cell leukemia/lymphoma (ATLL) patients, and present possible targets for future gene therapy.

1. Introduction

Interferons (IFNs) are multi-functional cytokines that regulate the genes involved in viral infection defense, immune system activation, hematopoietic development and modulation of cell growth. IFNs derive their effects through the transcriptional activation of target genes, which are regulated through IFN regulatory factors (IRFs). In mammals, the members of the IRF family of transcription factors (IRF-1–IRF-9) bind to the IFN-stimulated response elements (ISREs) found in the promoter regions of IFN-stimulated genes [1].

The expression of IRF-4 is restricted to the immune system, and is induced by diverse mitogenic stimuli, including T-cell receptor (TCR) cross-linking or treatment with phorbol-12-myristate-13-acetate (PMA)/Ionomycin (I) [2–4]. Mice deficient in the IRF-4 gene (IRF-$4^{-/-}$) exhibited profound defects in the functions of both B- and T-cells [5]. IRF-4 plays crucial roles in multiple steps of B-cell differentiation. For instance, IRF-4 activates the immunoglobulin light-chain genes by binding a specific DNA sequence in the 3′ enhancer regions, in cooperation with the ETS-family transcription factor PU.1, and by repressing the key germinal center regulator, BCL6 [6,7]. Recently, IRF-4 was reported to be the master regulator gene in multiple myeloma, a malignancy of plasma cells [7,8]. IRF-4 is also essential for several stages of T-cell and myeloid cell

Abbreviations: IRF-4, interferon regulatory factor-4; IFN, interferon; ISRE, IFN-stimulated response element; TCR, T-cell receptor; PMA, phorbol-12-myristate-13-acetate; I, Ionomycin; TAP, tandem affinity purification; IL-4, interleukin-4; HTLV-1, human adult T-cell leukemia virus type 1; ATLL, adult T-cell leukemia/lymphoma; NF-κB, nuclear factor-kappaB; NFATc2 (NFAT1), nuclear factor of activated T-cells; AZT, azidothymidine (zidovudine).

* Corresponding author. Tel./fax: +81 95 849 7001.
E-mail address: tosim@nagasaki-u.ac.jp (T. Matsuyama).

[1] Both authors contributed equally to this work.

1043-4666/$ - see front matter © 2011 Elsevier Ltd. All rights reserved.
doi:10.1016/j.cyto.2011.08.014

differentiation. We, as well as other groups, have found that, in the absence of IRF-4, not only the development of Th2 but also that of a cDC subset, $CD8\alpha^{-}CD11b^{+}$, is severely impaired [9–12]. The IRF-4 functions are regulated by several IRF-4-binding proteins. FK506-binding protein 52 (FKBP52) reportedly bound to IRF-4 in HTLV-1 (human T-cell leukemia virus type 1)-infected T-cells, and repressed the IRF-4 function by preventing the nuclear translocation and the target DNA binding of IRF-4 [13]. The IRF-4-dependent IL-4 induction in the presence of PMA and Ionomycin was enhanced by NFATc2 (NFAT1), and provided an important molecular function in T-helper cell (Th) differentiation [9]. NFATc1 (NFAT2) also activated the human IL-2 and IL-4 promoters in cooperation with IRF-4 [14]. Recently, it was reported that the elevated expressions of a nuclear factor-kappaB (NF-κB) family member, c-Rel, and IRF-4 are associated with the prognosis in adult T-cell leukemia/lymphoma (ATLL) patients [15]. To elucidate the mechanism, we isolated IRF-4-binding proteins from the HTLV-1-infected T-cells (HUT102), using the tandem affinity purification (TAP) method [16]. We identified c-Rel, as a novel IRF-4-associated protein in T-cells. We further examined whether IRF-4 activates the promoters of IL-2 (a T-cell growth factor) and IL-4 (an inducer of Th2 differentiation and growth) in cooperation with c-Rel in the stimulated T-cells.

2. Materials and methods

2.1. Cell culture and transfection

HUT102, an HTLV-1-infected human T-cell line, and EL-4, a murine thymoma cell line, were grown in RPMI 1640 medium supplemented with 10% heat-inactivated fetal bovine serum (FBS), and transfected with the indicated plasmids by electroporation using a pipette-type electroporator, Microporator MP-100 (Digital Bio). HEK293T cells were grown in 10% FBS-supplemented DMEM, and transfected with the indicated plasmids using the FuGENE 6 transfection reagent (Roche).

2.2. Plasmid constructs

The full-length human IRF-4 cDNA (1–1356) [2], and the PCR-amplified DNA fragments, (1–405) and (403–1356), were inserted downstream of the FLAG tag in the pcDNA3 vector (Invitrogen). The unique restriction enzyme, ApaI, was used to excise the N-terminal (1–1174) and C-terminal (1174–1860) regions from the full-length human c-Rel cDNA (1–1860) [17]. The fragments were inserted downstream of the HA tag in the pcDNA3 vector. The IL-4-Luc reporter plasmid was constructed by inserting the PCR-amplified promoter region (−250 to +15) of the human IL-4 gene into the pGL2-Basic vector (Promega). All constructs were confirmed by DNA sequencing.

2.3. Preparation of cell extracts

Cell lysates were prepared by vigorous vortexing in 400 μl of lysis buffer (20 mM Tris, pH 8.0, 150 mM NaCl, 1 mM EDTA, 1% NP40), containing a protease inhibitor mix (Boehringer), 48 h after transfection in a 6-well plate.

For the preparation of the nuclear extract, HUT102 cells (1×10^6 cells) were transfected with the indicated plasmids, and the nuclear proteins were extracted as described previously [18].

2.4. Immunoprecipitation and immunoblot analyses

The cell lysates were incubated with anti-FLAG M1 antibody-conjugated agarose beads (Sigma) for 2 h at 4 °C. The nuclear extracts from HUT102 cells were incubated with 5 μg of goat polyclonal anti-IRF-4 antibody (Santa Cruz Biotechnology), rabbit polyclonal anti-c-Rel antibody (Santa Cruz Biotechnology) or the corresponding control IgG antibody (Sigma), and Protein A Sepharose4B Fast Flow beads, for 3 h at 4 °C. The immunocomplexes were extensively washed, and the co-precipitated proteins were eluted from the Sepharose beads by boiling in SDS sample buffer. Each sample was resolved by SDS–PAGE, transferred to a PVDF membrane, and incubated with the indicated antibodies. Specific proteins were visualized with the appropriate HRP-conjugated antibodies and the ECL Plus detection system (Amersham Pharmacia Biotech).

2.5. Chromatin immunoprecipitation (ChIP)

The nuclear extracts from HUT102 cells were subjected to DNA–protein cross-linking with 1% formaldehyde for 5 min. After extensive washing, the samples were suspended in 500 μl of 150 mM NaCl, 25 mM Tris, pH 7.5, 5 mM EDTA, 1% Triton X-100, 0.1% SDS, and 0.5% deoxycholate, and were sonicated. After centrifugation at 14,000 rpm for 10 min at 4 °C, the supernatants were precipitated with 25 μg anti-IRF-4 antibody, anti-c-Rel antibody, or the corresponding IgG (Sigma) (as a control), and Protein A Sepharose4B Fast Flow beads. The amounts of precipitated DNA were quantified by PCR, using a pair of IL4 promoter-specific primers (Forward: 5′-CAAAGCAAAAAGCCAGCA-3′, Reverse: 5′-CGTTACACCAGATTGTCAGTCAC-3′).

2.6. Mice and primary T-cell activation

IRF-4 deficient ($IRF\text{-}4^{-/-}$) mice were initially mated to C57BL/6 mice, and were maintained by intercrossing in the Laboratory Ani-

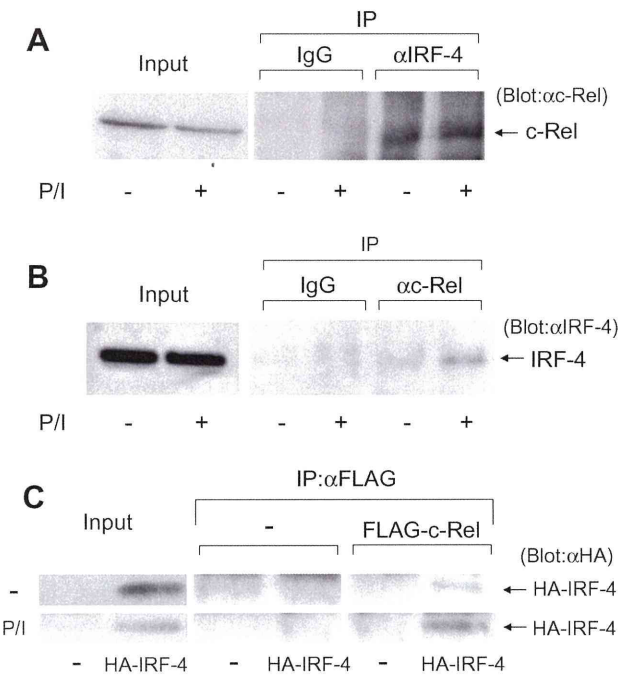

Fig. 1. IRF-4 and c-Rel binding. (A and B) Nuclear extracts from HUT102 cells (5×10^6), cultured for 8 h in the presence or absence of 250 ng/ml PMA and 1 μM Ionomycin (P/I), were immunoprecipitated with the IRF-4 antibody (A) or the c-Rel antibody (B). The SDS–PAGE fractionated proteins were blotted with the c-Rel antibody (A) and the IRF-4 antibody (B), respectively. (C) HEK293T cells (4×10^5) were transfected with an HA-tagged IRF-4 expression plasmid and/or Flag-tagged c-Rel expression plasmid (500 ng each), using the FuGENE reagent. Two days after transfection, the cells were incubated for 8 h in the presence or absence of P/I. The nuclear extracts were prepared, immunoprecipitated with an anti-FLAG antibody, and blotted with an anti-HA antibody.

mal Center for Animal Research at Nagasaki University. Mice were used at 5–6 weeks of age. The animal experiments reported herein were conducted according to the Guidelines of the Laboratory Animal Center for Biomedical Research at Nagasaki University.

Freshly isolated $CD4^+$ T-cells, from the spleens of C57BL/6 and IRF-$4^{-/-}$ littermates, were treated continuously with TNF-α (5 ng/ml) for 6 h. The cells were then collected by centrifugation and cultured at a density of 1×10^6 cells/ml in six-well plates precoated with anti-TCRβ mAb (H57–597, 10 μg/ml). Cells were harvested at 4 h for RNA analyses.

2.7. RNA isolation and reverse-transcription PCR

Total RNA was extracted from the $CD4^+$ T-cells and the HUT102 cells transfected with the indicated plasmids, using Isogen (Nippon Gene, Japan). cDNA was generated from 1 μg RNA, using reverse transcriptase. The PCR primers used for human IL-2 were 5′-TGTACAGCATGCAGCTCGC-3′ and 5′-TGCTTCCGCTGTAGAGCTTG-3′, those for mouse IL-2 were 5′-GAGTCAAATCCAGAAGATGCCGCAG-3′ and 5′-TGATGGACCTACAGGAGCTCCTGAG-3′, those for mouse IL-4 were 5′-CGAAGAACACCACAGAGAGTGAGCT-3′ and 5′-GACTCATTCATGGTGCAGCTTATCG-3′, those for G3PDH were 5′-CATCTGAGGGCCCACTGAAG-3′ and 5′-TGCTGTTGAAGTCGCAGGAG-3′, those for human β-actin were 5′-AAGAGAGGCATCCTCACCCT-3′ and 5′-TACATGGCTGGGGTGTTGAA-3′, and those for mouse β-actin were 5′-TGGAATCCTGTGGCATCCATGAAAC-3′ and 5′-TAAAACGCAGCTCAGTAACAGTCCG-3′.

2.8. Intraperitoneal injections and cell isolation

Complete and incomplete Freund's adjuvants (CFA/IFA) were purchased from Difco Laboratories. An emulsion (100 μl) of CFA in PBS was injected into each of the C57BL/6 and IRF-$4^{-/-}$ littermates, followed by an injection of 100 μl of IFA on the next day. PBS alone was used as a negative control for all experiments. The animals were sacrificed on day 6. Lymphocytes were collected from the spleens. Total $CD4^+$ T-cells were purified using magnetic particles conjugated with anti-CD4 Ab (Imag Cell Separation

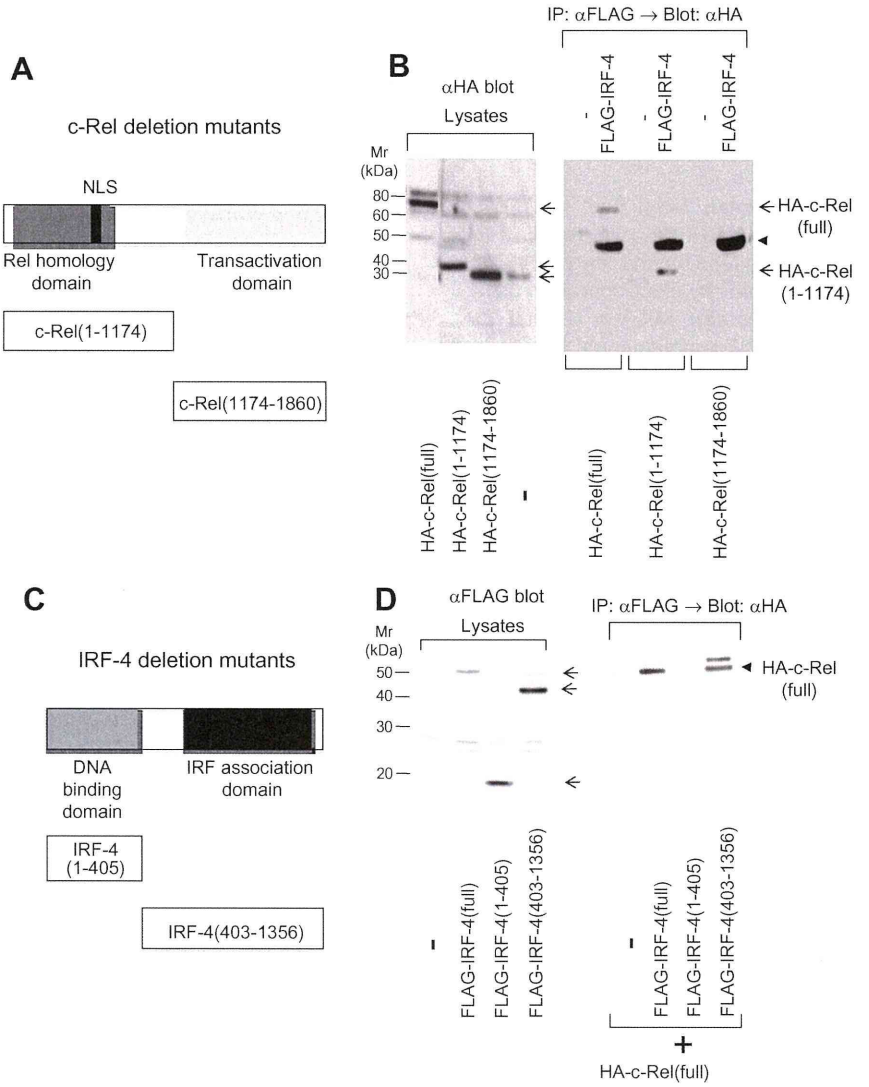

Fig. 2. Determination of IRF-4 and c-Rel binding sites. (A and B) HA-tagged full-length, N-terminal half (1–1174), and C-terminal half (1174–1860) c-Rel constructs (500 ng each) were introduced with FLAG-tagged full-length IRF-4 (500 ng) into 4×10^5 HEK293T cells in 6-well plates. The lysates (B, left panel), and the c-Rel deletion mutants co-immunoprecipitated with IRF-4 by the anti-FLAG antibody (B, right panel) were detected with an anti-HA antibody. The arrows indicate the HA-c-Rel bands, and the arrowhead shows a non-specific band. (C and D) FLAG-tagged full-length, N-terminal region (1–405), and C-terminal region (403–1356) IRF-4 constructs (500 ng each) were introduced with HA-tagged full-length c-Rel (500 ng) into 4×10^5 HEK293T cells in 6-well plates. The lysates (D, left panel), and the c-Rel co-immunoprecipitated with the IRF-4 deletion mutants by the anti-FLAG antibody (D, right panel), were probed with an anti-HA antibody. The arrows and arrowhead indicate the FLAG-IRF-4 bands, and the HA-c-Rel band, respectively.

System, BD Biosciences), as specified by the manufacturer. This protocol provided cells with >99% purity, as assessed by flow cytometry. Freshly isolated $CD4^+$ T-cells were collected by centrifugation and cultured at a density of 1×10^6 cells/ml in six-well plates precoated with various concentrations of anti-TCRβ mAb (H57–597). Cells were harvested at 16 h for cytokine assays, using sandwich ELISA. For the mRNA preparation, the isolated $CD4^+$ T-cells (2×10^5 cells/well) were stimulated in the 96-well paltes precoated with the indicated concentrations of anti-CD3 (Pharmingen) and anti-CD28 (Southern Biotech) antibodies for 4 h.

3. Results

3.1. Identification of the proteins associated with IRF-4 by the TAP method, followed by mass spectrometry

To identify the proteins that associate with IRF-4 in T-cells, we purified the IRF-4-binding complex by the TAP method, as described previously [16], and in Supplemental Figs. 1S–3S. We excised 30 well-separated bands that were specifically bound to IRF-4 from the gel, digested them with trypsin, and identified them by tandem mass spectrometry. However, only fourteen bands, in addition to IRF-4, were identified with significant scores ($p < 0.05$) in the Swiss-Prot database, using the MASCOT search engine (Supplemental Table S1). One of the peptide sequences acquired from the approximately 75–80 kDa protein band was matched to the human c-Rel proto-oncogene protein.

3.2. Specific binding between IRF-4 and c-Rel

We further analyzed the binding of c-Rel to IRF-4, because the enhanced expression of both c-Rel and IRF-4 is associated with the prognosis in ATLL patients [15,16]. An HTLV-1 (human T-cell leukemia virus type 1)-infected T-cell line, HUT102, also expresses large amounts of IRF-4 and c-Rel. As shown in Fig. 1A, the IRF-4 antibody co-precipitated c-Rel with IRF-4 more effectively in the presence of 250 ng/ml PMA and 1 μM Ionomycin (P/I), as compared to the control IgG. Conversely, the anti c-Rel antibody also co-precipitated IRF-4 with c-Rel independently of the P/I treatment, as compared to the control IgG (Fig. 1B). Since the amounts of IRF-4 and c-Rel were not affected by the P/I treatment, the enhanced binding by P/I indicated that the P/I treatment induced a functional change in IRF-4, c-Rel, or other binding molecules. In addition, we examined whether IRF-4 directly binds to c-Rel, by over-expressing them in HEK293T cells. The HA-tagged IRF-4 was specifically co-precipitated with the FLAG-tagged c-Rel, and the binding was enhanced in the presence of P/I (Fig. 1C).

Next, we examined the region of c-Rel that is responsible for its interaction with IRF-4, using HA-tagged deletion mutants of c-Rel (Fig. 2A and B). The expected 68-kDa, 39-kDa, and 34-kDa bands for the full-length, N-terminal half (1–1174), and C-terminal half (1174–1860) c-Rel constructs, respectively, were detected with an anti-HA antibody (Fig. 2B, left). Each mutant c-Rel was co-expressed with FLAG-tagged IRF-4 in HEK293T cells and subjected to an immunoprecipitation assay. As shown in the right panel of Fig. 2B, the full-length and the N-terminal half (1–1174) c-Rel constructs interacted with IRF-4, in contrast to the C-terminal half (1174–1860). A strong band was detected always in the lanes containing FLAG-IRF-4. This may be related to IRF-4, however, the binding of the N-termial half c-Rel to IRF-4 was specific, because the C-terminal half c-Rel was not co-precipitated with FLAG-IRF-4 using the anti-FLAG antibody. On the other hand, the FLAG-tagged full-length and the C-terminal IRF association domain (403–1356) of the IRF-4 constructs co-precipitated HA-tagged c-Rel, in contrast to the N-terminal DNA binding domain (1–405)

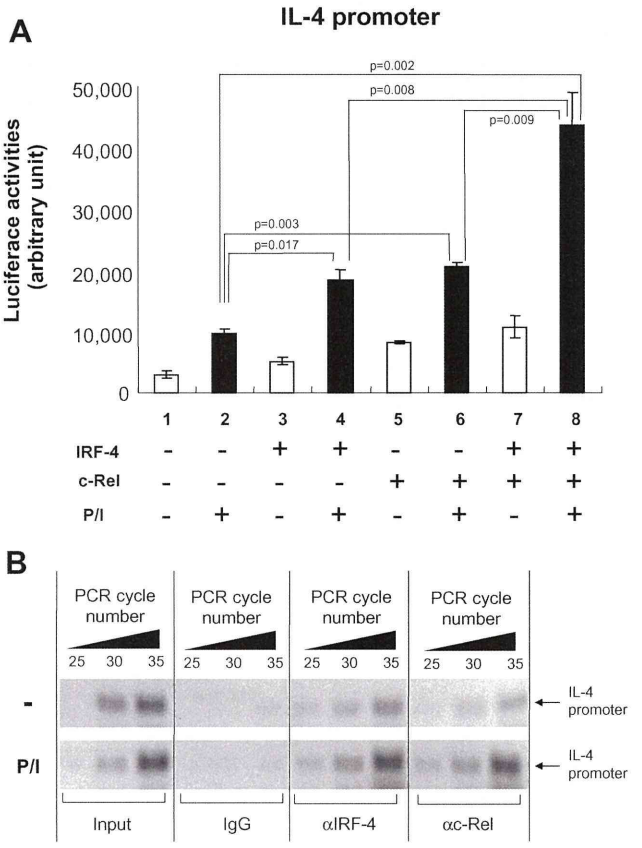

Fig. 3. IRF-4 and c-Rel co-operatively activate the human IL-4 promoter. (A) HUT102 cells (2×10^5) were transfected with a luciferase reporter construct driven by the human IL-4 promoter (−250 to +15) (1 μg) with/without IRF-4, and c-Rel expression plasmids (200 ng each) by electroporation. Two days after transfection, the cells were incubated for 8 h in the presence or absence of 250 ng/ml PMA and 1 μM Ionomycin (P/I), and the luciferase activities were measured. Results show the mean ± SE of three independent experiments. (B) The chromatin immunoprecipitation (ChIP) assay was performed using HUT102 cells (5×10^6) treated with/without P/I for 8 h, with anti-IRF-4 and anti-c-Rel antibodies. The amount of specifically precipitated DNA was determined semi-quantitatively, by changing the PCR cycle numbers (25, 30 and 35 cycles) with primers specific for the IL4 promoter (−300 to −80).

of IRF-4 (Fig. 2C and D). These results indicated the interaction between the N-terminal half of c-Rel, containing the Rel homology domain, and the C-terminal IRF association domain of IRF-4.

3.3. IRF-4 and c-Rel cooperatively activate the IL-4 promoter

To explore the effects of c-Rel on the IRF-4 functions *in vivo*, we first examined the effects of c-Rel on the IRF-4-dependent IL-4 stimulation in HUT102 cells, using a luciferase reporter assay with an IL-4 promoter, because IRF-4 reportedly stimulated IL-4 expression via a physical interaction with NFATc2 and/or NFATc1 [9,14]. As shown in Fig. 3A, the P/I treatment enhanced the basal IL-4 promoter activities (the open vs. filled bars), and the IRF-4 (lane 4), c-Rel (lane 6), and IRF-4 + c-Rel (lane 8) activities were significantly enhanced by 1.88 ± 0.18-, 2.11 ± 0.07-, and 4.47 ± 0.55-fold, respectively, as compared to the basal IL-4 promoter (lane 2). Next, we tested the binding of IRF-4 and c-Rel to the IL-4 promoter region, using a ChIP assay. The amounts of the IRF-4 promoter region (−300 to −80) that co-precipitated with the anti-IRF-4, c-Rel, and control antibodies were determined semi-quantitatively, by changing the PCR cycle numbers (25, 30, and 35 cycles) in the presence or absence of P/I treatment (Fig. 3B). The specific binding of IRF-4 and c-Rel to the IL-4 promoter region was observed, and